## 3. EXAMPLE OF CALCULATION

A numerical example relative to the design and verification of a pultruded frame subjected to static and seismic actions is illustrated (see Figure 3.1). The procedure will be the same also in presence of different structures as simple frame, multistory frame or irregular structure all made by beam-column connections or, again, for local reinforcement using pultruded FRP systems.

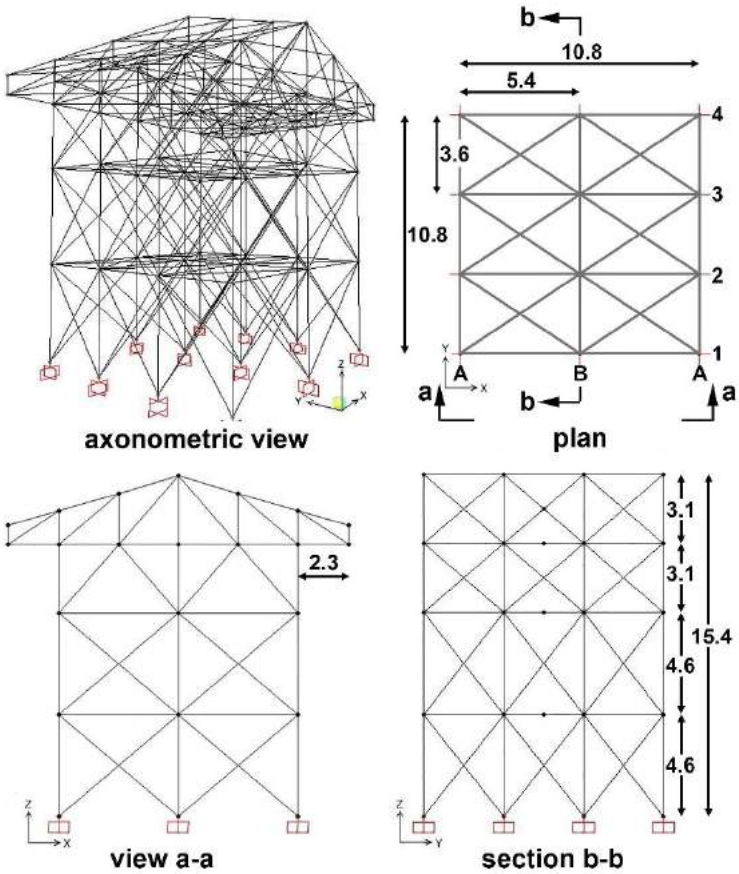


Figure 3.1 View of structure (dimensions in meters).

In this first part of the chapter, the characteristics of the structure are described and general indications are given about the seismic behavior and design of pultruded frames.

In the second part of the chapter, Load analysis (p. 42), the static and seismic loads acting on the structure are evaluated. The seismic response of the building is evaluated first through a spectral response analysis and then through a pushover analysis.

The third part of the chapter, from page 55, describes some structural verifications of the single members at the ultimate (ULS) and serviceability limit state (SLS). In addition, a verification of a bolted joint is carried out, considering the different failure mechanisms.

In particular, for what concerns the ULS and SLS, the following verifications are considered (Table 3.1):

| **Ultimate Limit State, ULS** | | **Serviceability Limit State, SLS** | |
|---|---|---|---|
| Example of verification of a compressed member | p. 59 | Stresses<br>Deformations | p. 76<br>p. 77 |

Table 3.1 Chapters of ULS and SLS verifications

For what concerns the verifications of joints the following verifications are considered (Table 3.2):

| **Joint's verification** | |
|---|---|
| Net-tension failure of the plate | p. 82 |
| Shear-out failure of the plate | p. 82 |
| Bearing failure of the plate | p. 83 |
| Shear failure of the steel bolt | p. 85 |

Table 3.2 Chapters of joint verifications

On the base of the verifications results some considerations about the structural performance of pultruded members are then provided. Finally, the possible strategies are described for enhancing the seismic stability of the structures.

## 3.1. **Statement of the structural design**

The structure of Figure 3.1 has been designed in accordance with the Italian building code (NTC08) and Eurocode. Individual components (frames, members, connections and bolted joints) and the whole structure have been analyzed with respect to Ultimate Limit States (ULS) and Serviceability Limit States (SLS). The adopted design method takes into account the load combinations of wind, snow and earthquake. Seismic loading was based on seismic zoning in accordance with the Italian Building Code NTC08 (2008).

The structure has been designed for a design working life $V_N \geq 50$ years (see also Eurocode1 category C and NTC08 type 2 class III).

The referred life's period $V_R$ is so assumed equal to 75 years by the product between $V_N$ and $C_U$ (class of use) =1.5.

The parameters to identify the structures are the fundamental period of vibration T1 and the beam-column stiffness ratio $\rho$, equation 3.1(Chopra 2007):

$$\rho = \frac{\sum_{beams} \frac{EJ_b}{L_b}}{\sum_{columns} \frac{EJ_c}{L_c}} \tag{3.1}$$

with the flexural stiffness of beam ($EJ_b$) and column ($EJ_c$) compared to $L_b$ (lengths of beam) and $L_c$ (lengths of column) indicated in Figure 3.2.

The different $\rho$ value affects the fundamental period and the modal shapes. The relative closeness or separation between the natural periods and the corresponding participation mass evidences the global or local structural response.

The deflected shapes in function of $\rho$ values are indicated in Figure 3.2:

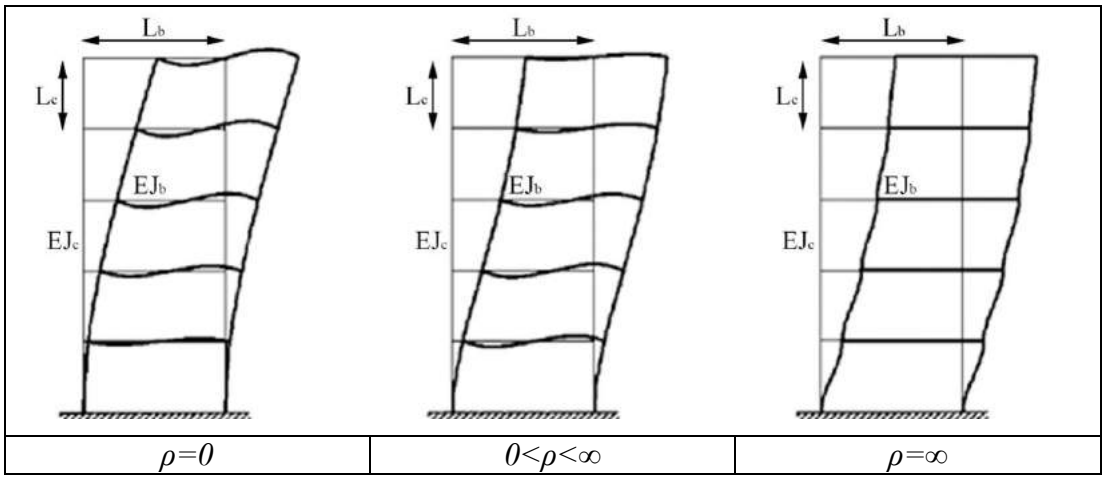


| $\rho=0$ | $0<\rho<\infty$ | $\rho=\infty$ |
|---|---|---|

Figure 3.2 Deflected shapes with different $\rho$; (Chopra 2007)

With $\rho=0$ the frame is not restrained on joint rotations, then the behaviour of the frame is affected by the flexural response of the beams. When $0<\rho<\infty$ (semi-rigid joints) beams and columns are subjected to bending deformation with joint rotations. With $\rho=\infty$ (rigid joints) the joint rotation is completely restrained.

In general, the connections between pultruded structural members can be realized through bolted or bonded joints or a combination of the two.

All-FRP structures should be designed also evaluating local and global buckling and their designing in function of the lower value.

As reported in EN 1998-1, §6.7.1, the concentric braced frames should be designed so that the strength hierarchy criteria are activated.

The structure should exhibit similar global load-deflection characteristics at each story in opposite senses of the same braced direction under load reversals. For this reason the diagonal elements of bracings should be placed as shown in Figure 3.3 (see Figure 6.12 of EN 1998-1).

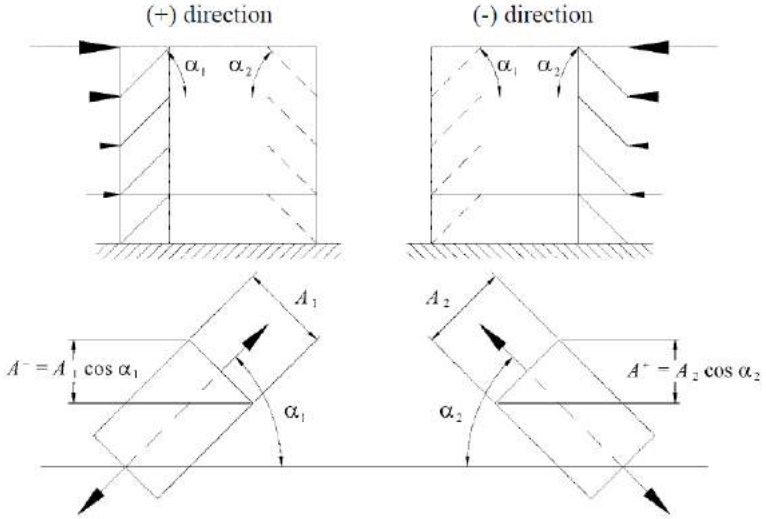


Figure 3.3 Figure 6.12 of EN 1998-1.

To this end, the equation 3.2 should be met at every story in order to concentrate the axial load in the bracings unloading the much as possible columns and beams.

$$\frac{\left|A^+ - A^-\right|}{A^+ + A^-} \le 0.05 \tag{3.2}$$

where $A^+$ is the area of the horizontal projection of the cross-section of tension diagonals with positive seismic action; $A^-$ is the area of the horizontal projection of the cross-section of tension diagonals with negative seismic action.

The effects of connections deformations on global drift must be taken into account using pushover global analysis or non-linear time history analysis, see Sheet 8 and Priestley et al. (2007).

As suggested by EN 1998-1:2004 the dissipative semi-rigid and/or partial strength connections are permitted if: 1-the connections have a rotation capacity consistent with the global deformations; 2-members framing into the connections are demonstrated to be stable at ULS; 3-the effect of connection deformation on global drift is taken into account using non-linear global analysis or non-linear time history analysis.

## 3.2. **Materials**

Table 3.3 shows the mechanical properties for the pultruded profiles with vinylester based matrix reinforced by E-glass fibre.

| Mechanical properties | Symbol | Mean value |
|---|---|---|
| Longitudinal tensile strength | $\sigma_Z = \sigma_{Lt}$ | 400 MPa |
| Longitudinal compressive strength | $\sigma_{Zc} = \sigma_{Lc}$ | 220 MPa |
| Transversal tensile strength | $\sigma_{Xt} = \sigma_{Yt} = \sigma_{Tt}$ | 70 MPa |
| Shear strength | $\tau_{XY} = \tau_{XZ} = \tau_{YZ}$ | 40 MPa |
| Longitudinal elastic modulus | $E_{Z=} E_L$ | 23 GPa |
| Transversal elastic modulus | $E_X = E_Y = E_T$ | 7 GPa |
| Shear modulus | $G_{XY} = G_L$ | 4.5 GPa |
| Shear modulus | $G_{ZX} = G_{ZY=} G_T$ | 4.5 GPa |
| Poisson's ratio | $\nu_{ZX} = \nu_{ZY} = \nu_L$ | 0.3 |
| Poisson's ratio | $\nu_{XY=} \nu_T$ | 0.3 |
| Bulk weight density of FRP | $\gamma$ | 1850 kg/m$^3$ |
| Volume fraction of E-glass fibre | $V_f$ | 48% |

Table 3.3 Mechanical and physical characteristics of pultruded FRP material, mean value

To assemble the whole FRP structure the use of stainless steel bolts will be suggested. For the frame joints the bolting is M14 class 8.8, UNI5737.

The bolt clearance hole should be constant at 1.0 mm. The M14 bolts should be tightened to a torque where the effects will be less than the transversal tensile strength. From the torque moment $M$ it is possible to detect the axial load $N$ through the Equation 3.3.

$$N = \frac{M}{\varsigma \cdot d} \tag{3.3}$$

where $d$ is equal to the diameter of the bolt while $\varsigma$ is a coefficient friction ($\varsigma$ = 0.14 to 0.22, Mottram et al. 2004). Bolts should be partially threaded (at least for half length of bolt) to minimise any local damage from thread embedment into the FRP materials.

## 3.3. **Basic assumptions**

The structure has been designed taking into account the following basic assumptions:

- full fixed restraint at column-base

- rigid diaphragm as horizontal partition

- for the material of bracing the constitutive law of Figure 3.4a has been considered that takes into account the partial cross section area due to presence of holes for bolted connection. The normalized constitutive law and the idealized curve for FEM analysis are reported in Figure 3.4b.

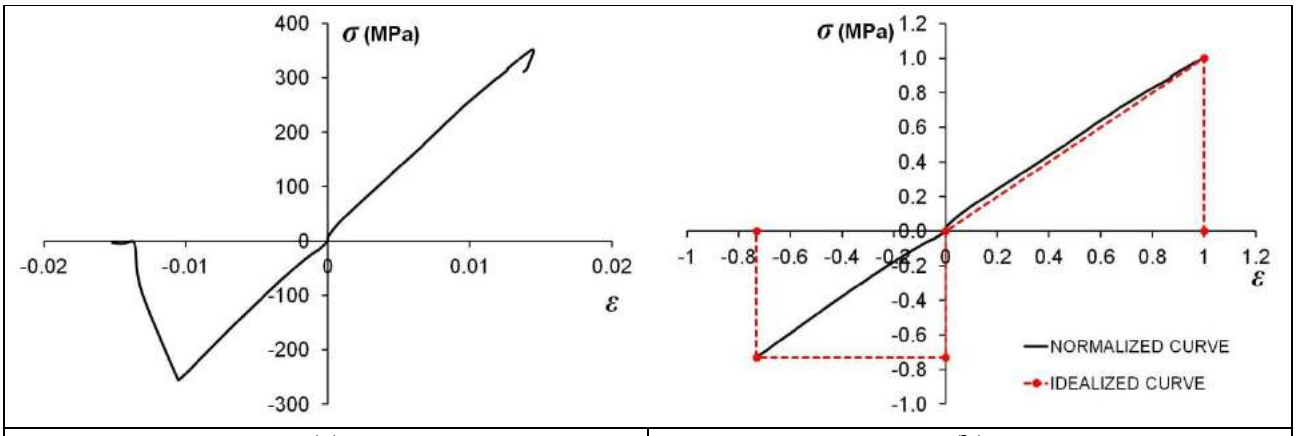


(a) (b)

Figure 3.4 Experimental and normalized constitutive law for the bracing elements

- for the beam-column joints the constitutive law of Figure 3.5 has been assumed. The moment-rotation relationship (Figure 3.5a) has been extracted by experimental tests carried out in the Laboratory of Strenght of Materials of IUAV Univesity of Venice, Italy (Feroldi and Russo 2016). The normalized constitutive law and the idealized curve for FEM analysis are reported in Figure 3.5b; other constitutive laws can be deduced by Turvey and Cooper (2004).

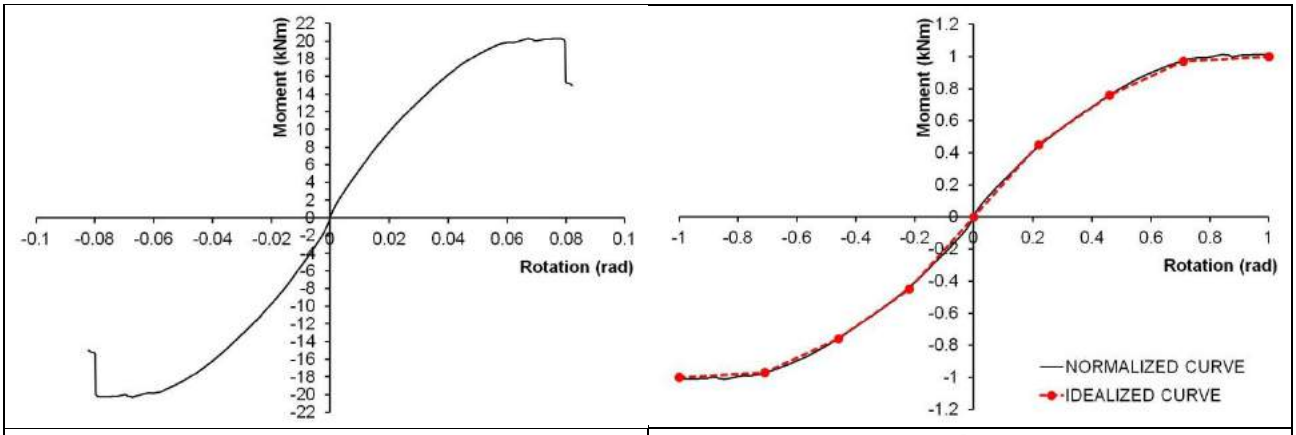


(a) (b)

Figure 3.5 Experimental and normalized Moment-Rotation relationship

## 3.4. **Load analysis**

For the ultimate and serviceability limit states, ULS and SLS respectively, the combinations of actions are listed in Table 3.4

| | |
|---|---|
| fundamental combination in ULS | $\gamma_{G1} \cdot G_1 + \gamma_{G2} \cdot G_2 + \gamma_{Q1} \cdot Q_{k1} + \gamma_{Q2} \cdot \psi_{02} \cdot Q_{k2} + \gamma_{Q3} \cdot \psi_{03} \cdot Q_{k3} + ...$ |
| characteristic combination in SLS | $G_1 + G_2 + Q_{k1} + \psi_{02} \cdot Q_{k2} + \psi_{03} \cdot Q_{k3} + ...$ |
| frequent combination in SLS | $G_1 + G_2 + \psi_{11} \cdot Q_{k1} + \psi_{22} \cdot Q_{k2} + \psi_{23} \cdot Q_{k3} + ...$ |
| quasi-permanent combination in SLS | $G_1 + G_2 + \psi_{21} \cdot Q_{k1} + \psi_{22} \cdot Q_{k2} + \psi_{23} \cdot Q_{k3} + ...$ |
| seismic combination in ULS | $E + G_1 + G_2 + \psi_{21} \cdot Q_{k1} + \psi_{22} \cdot Q_{k2} + ...$ |

Table 3.4 Combination of actions

where $G_1$ and $G_2$ are the dead loads of the structural and non structural elements respectively, $Q$ is the accidental load and $E$ is the seismic action.

The recommended values of $\psi$ factors for buildings (Table 3.5) are extracted by Table A1.1 for Eurocode 1 and Table 2.5.1 for NTC08.

| **Action/Category** | $\Psi_{0j}$ | $\Psi_{1j}$ | $\Psi_{2j}$ |
|---|---|---|---|
| Category C: congregation areas | 0.7 | 0.7 | 0.6 |
| Snow load on building for sites located at altitude H≤1000 m a.s.l. | 0.5 | 0.2 | 0 |
| Wind loads on buildings | 0.6 | 0.2 | 0 |

Table 3.5 Recommended values for $\psi$ coefficients

For the ULS the design values of actions are shown in Table 3.6, see Tables A1.2(B) and A1.2(C) for Eurocode 1 and Table 2.6.1 for NTC08

| **Loads/Actions** | $\gamma_F$ | |
|---|---|---|
| Permanent | $\gamma_{G1}$ | 1.3, 1.5 |
| Permanent | $\gamma_{G2}$ | 1.5 |
| Variable | $\gamma_{G2}$ | 1.5 |

Table 3.6 Unfavourable condition of design values of actions

### 3.4.1. **Permanent loads**

The total self-weight of structural and non-structural members should be taken into account in the combinations of actions as a single action.

The scheme of the structure is indicated in Figure 3.6. Along X and Y-direction the frames 1-2-3-4 and A-B are shown, respectively. The horizontal bracing in the plan scheme of Figure 3.6 is repeated for every floor. The details of cross sections of pultruded members of the structure (Figure 3.1) are shown in Figures 3.6 and 3.7, while Table 3.7 lists the main geometric characteristics.

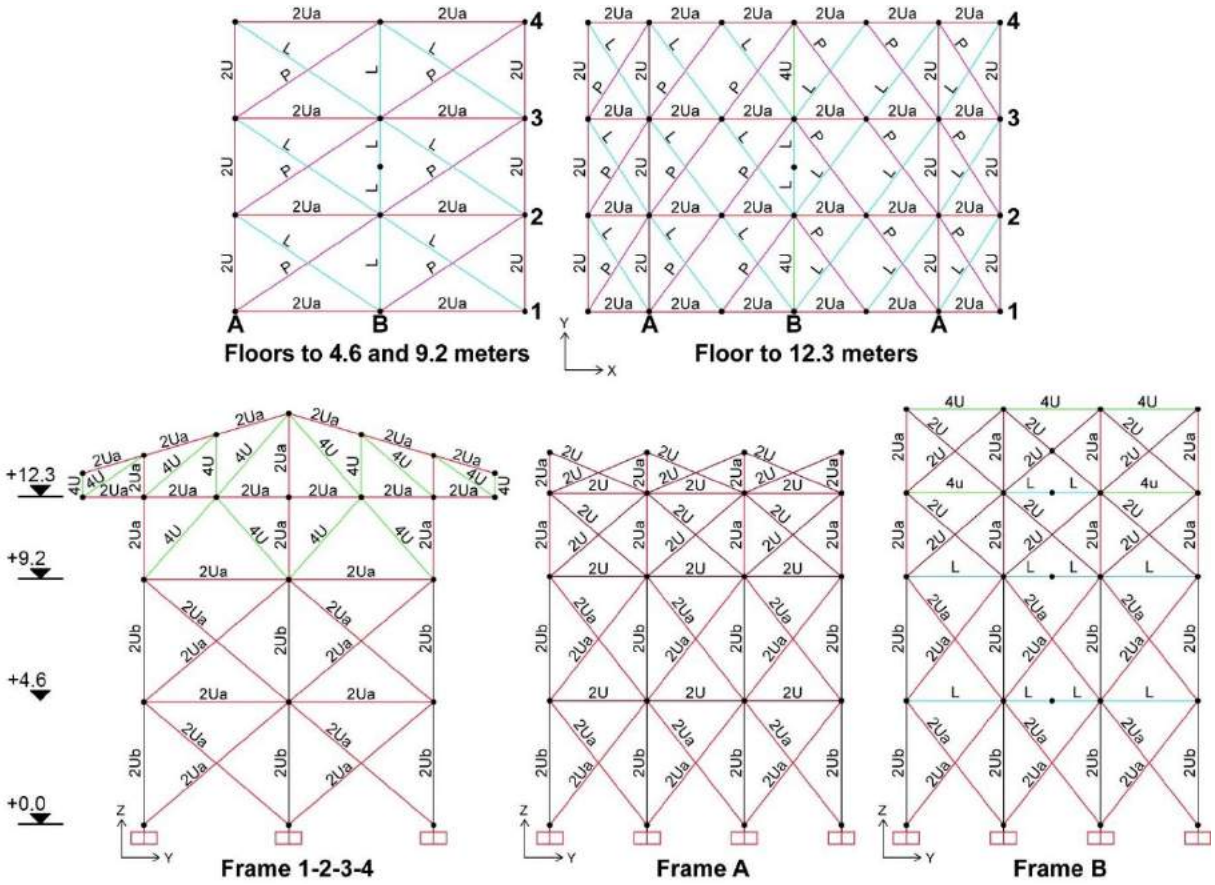


Figure 3.6 Details of members for every floor and frame (meters)

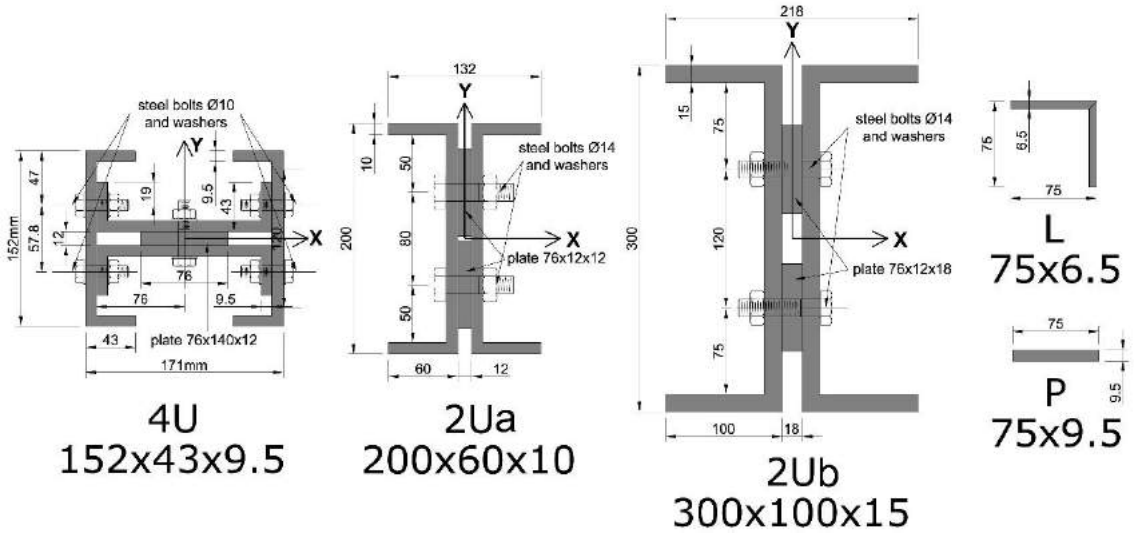


Figure 3.7 Geometric characteristics of cross section members (millimetres)

| Section name | Area | Second moment of inertia $I_{max}$ | Second moment of inertia $I_{min}$ | Torsional second moment of inertia | Shear area for $I_{max}$ | Shear area for $I_{min}$ |
|---|---|---|---|---|---|---|
| | $mm^2$ | $mm^4$ | $mm^4$ | $mm^4$ | $mm^2$ | $mm^2$ |
| 2U-152x43x9.3 | 4080.84 | 11834397 | 1975906 | 108225.2 | 2827.2 | 1599.6 |
| 2U-200x60x10 | 6000 | 31400000 | 4687500 | 187400 | 4000 | 2400 |
| 2U-300x100x15 | 14100 | 1.71E+08 | 26811875 | 993712.5 | 9000 | 6000 |
| 4U-152x43x9.3 | 8162 | 31829200 | 13809900 | 232400 | 7112 | 3196 |
| L-75x6.5 | 932.75 | 503065.6 | 503065.6 | 12698.89 | 487.5 | 487.5 |
| P-75x9.5 | 712.52 | 334004.9 | 5359.02 | 16303.56 | 712.5 | 180.52 |

Table 3.7 Characteristics of pultruded FRP members

A composite cross section constituted by pultruded panels and concrete slab has been considered in addition to $G_1$ for every floor and the roof. In detail, the pultruded panels have a self-weight of 0.5kN/m$^2$ with a thickness of 80mm, while the concrete slab is 100 mm thick, see Figure 3.8.

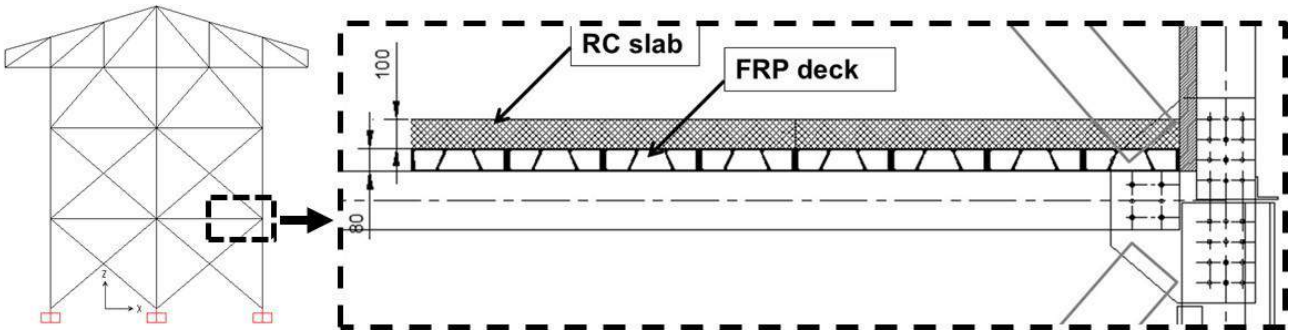


Figure 3.8 Detail of deck (millimetres)

The permanent load $G_1$ weighing on beams with maximum span for every floor and on the beam of the roof is shown in Figure 3.9, for the references about the frames see Figure 3.6.

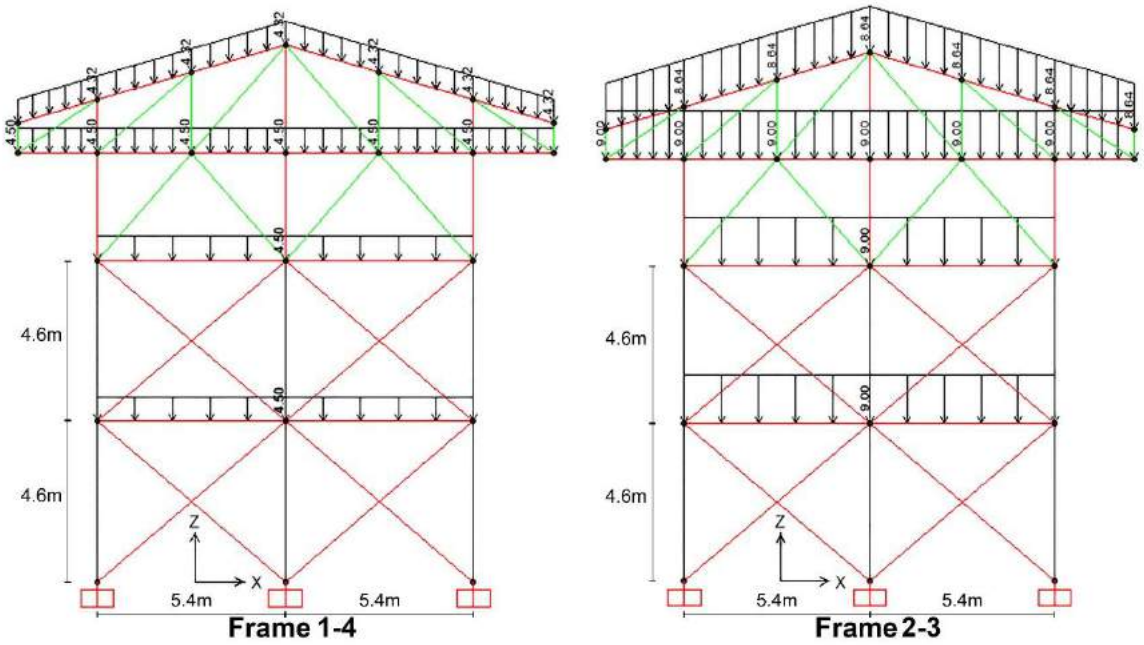


Figure 3.9 Permanent load $G_1$ (N/mm)

$G_2$ is characterized by non-structural permanent load as infill vertical panels, internal partitions and layer of pavement, see Figure 3.10; for the references of the frames see Figure 3.6.

In detail, the load of non-structural layer of pavement and internal partitions is equal to 3.8 kN/m$^2$ while the load of perimetral infill vertical panel is 0.5 kN/m$^2$.

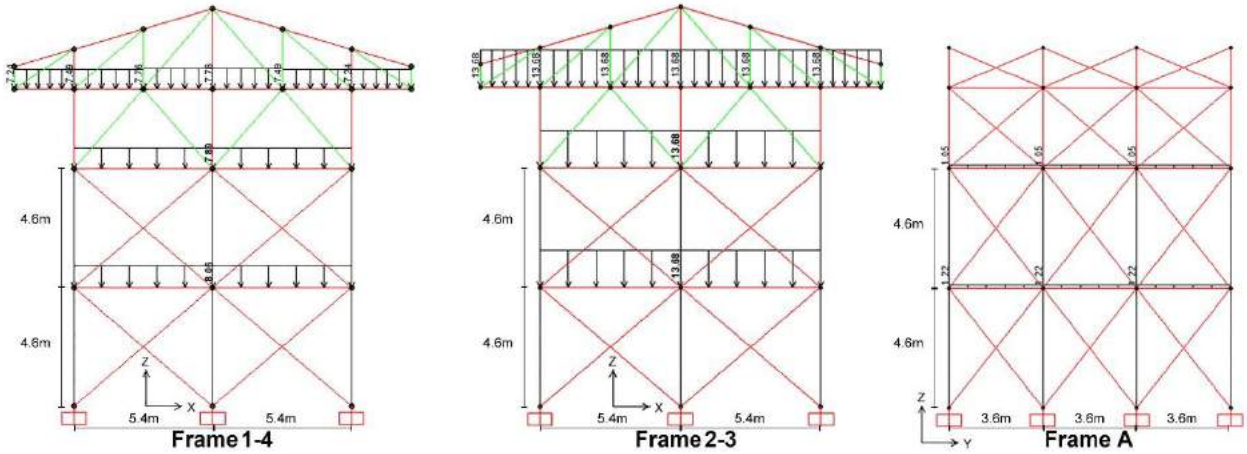


Figure 3.10 Non-structural permanent load $G_2$ (N/mm)

### 3.4.2. **Variable loads**

The variable action $Q$ on building floor is 4 kN/m$^2$, weighing on beams with maximum span (see Figure 3.1) as shown in Figure 3.11; for the references about the frames see Figure 3.6.

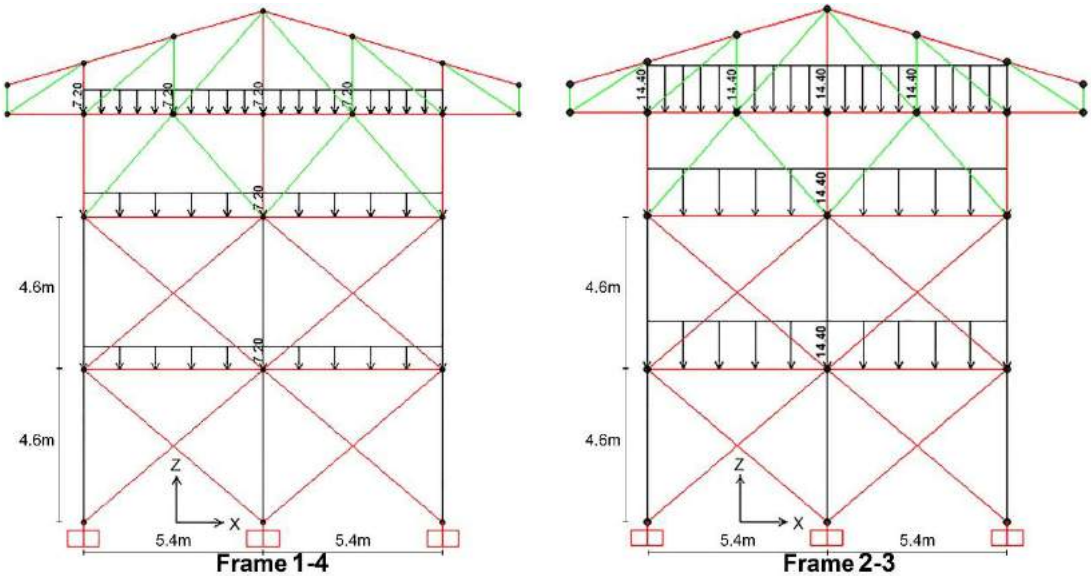


Figure 3.11 Variable actions $Q$ load (N/mm)

The wind action has been evaluated considering the characteristics of the Zone 3 in NTC08 (Table 3.3.I of §3.3). The fundamental value of the basic wind velocity, $v_{b,0}$, is obtained by the following relationship:

$$v_b = v_{b,0} + k_a(a_s - a_0) \text{ for } a_0 < a_s < 1500m$$

$$v_b = 27 + 0.02 \cdot (783 - 500) = 32.66 \frac{m}{\sec}$$

where $v_{b,0}$, $a_0$, $k_a$, are parameters listed in Table 3.3.I of §3.3 of NTC08 while $a_s$ is the altitude above the sea level. The velocity pressure $p$ is given by:

$$p = q_b \cdot c_e \cdot c_p \cdot c_d$$

with $c_e$=exposure factor, $c_p$=shape parameter, $c_d$=dynamic coefficient=1, while the basic velocity pressure $q_b$ is calculated through

$$q_b = \frac{1}{2} \cdot \rho \cdot v_b^2$$

where $\rho$ is the air density equal to 1.25kg/m$^3$, then

$$q_b = \frac{1}{2} \cdot 1.25 \cdot (32.66)^2 = 666.67 \frac{N}{m^2}$$

for the exposure factor $c_e$ the following relationship must be applied

$$C_e(z) = k_r^2 \cdot C_t \cdot \ln\left(\frac{z}{z_0}\right) \cdot \left[7 + C_t \cdot \ln\left(\frac{z}{z_0}\right)\right]$$

where for the category III $k_r$, $z_0$ and $z$ are listed in Table 3.3.II of NTC08 while $C_t$ is equal to topographic coefficient =1 , hence:

$$C_e(z) = (0.2)^2 \cdot 1 \cdot \ln\left(\frac{15.4}{0.1}\right) \cdot \left[7 + 1 \cdot \ln\left(\frac{15.4}{0.1}\right)\right] = 2.42$$

For the shape parameter, $c_p$, the net pressure is the difference between the pressures on the opposite surfaces that in this specific case is $c_p$ = 1.2. Finally, the velocity pressure $p$ is detailed in Figure 3.12.

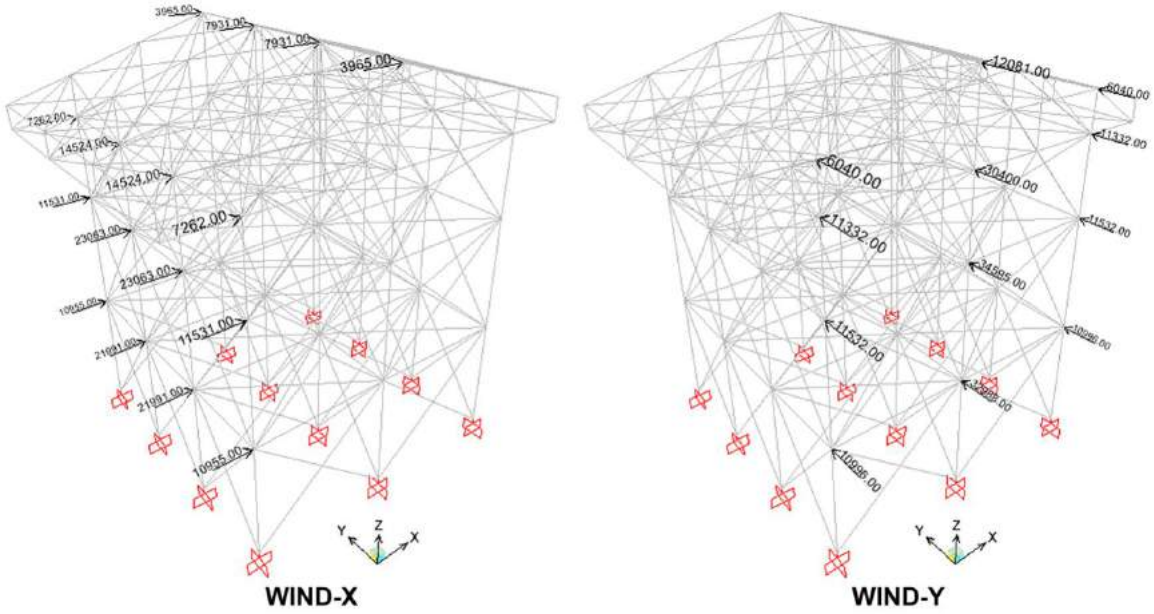

Figure 3.12 Wind actions in X and Y-direction, force in N

The snow load, as defined by NTC08 and EC1, is shown in the following relationship.

$$q_s = \mu_1 \cdot q_{sk} \cdot C_E \cdot C_t$$

Where $q_s$ ($S$, for EC1) = snow load, $\mu_i$ = shape coefficient, $C_E$ = exposure coefficient, $C_t$ = thermal coefficient and $q_{sk}$ ($S_k$ = permanent and $S_{Ad}$ = variable, for EC1) = characteristic value. The different parameters are listed in Table 3.8. Figure 3.13 shows the snow load applied to structure; for the references of the frames see Figure 3.6.

| | $\mu_i$ | $C_E$ | $C_t$ | $q_{sk}$ ($S_k$=permanent, for EC1) | $q_{sk}$ ($S_{Ad}$=variable, for EC1) |
|---|---|---|---|---|---|
| EC1 | 0.8 | 1.1 | 1 | $S_k = (0.498-0.209)\left[1+\left(\frac{A}{452}\right)^2\right] =$ $(0.498-0.209)\left[1+\left(\frac{783}{452}\right)^2\right] = 3.15\frac{kN}{m^2}$ | $S_{Ad} = C_{esl} \cdot S_k = 2 \cdot 3.148 = 6.296\frac{kN}{m^2}$ |
| NTC08 | 0.8 | 1.2 | 1 | $q_{sk} = 0.51 \cdot \left[1+\left(\frac{a_s}{481}\right)^2\right] = 1.86\frac{kN}{m^2}$ (with $a_s$=783) | |

Table 3.8 Coefficients for snow load

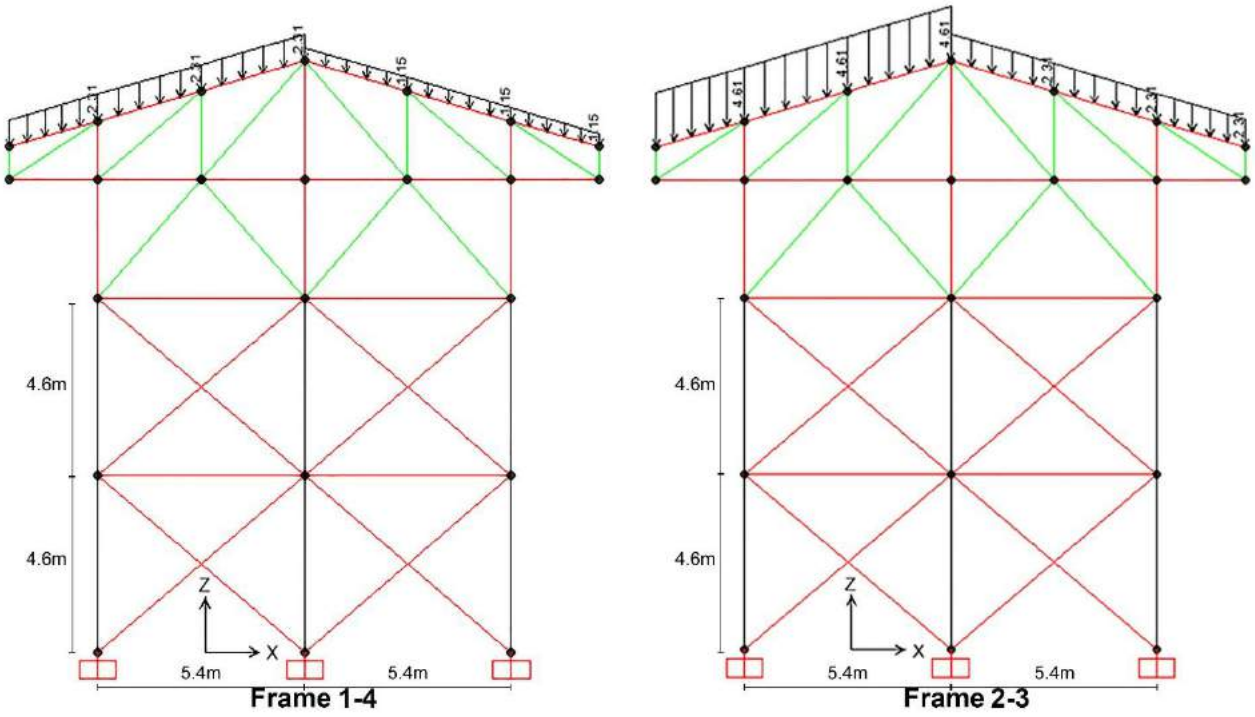


Figure 3.13 Snow load (N/mm)

### 3.4.3. **Seismic analysis**

A dynamic analysis has been carried in the following taking into account the modal analysis, spectral analysis and non linear static analysis.

#### 3.4.3.1. **Modal analysis**

The modal analysis, associated with the design response spectrum, can be performed on three-dimensional structures in order to obtain a reliable structural response.

This is a linear dynamic-response procedure which evaluates and superimposes free-vibration mode shapes to characterize displacement patterns. Mode shapes describe the configurations into which a structure will naturally displace in the dynamic field.

Typically, lateral displacement patterns are of primary concern. The analysis can be considered reliable as it reaches the mass participant >85% (§7.3.3.1 of NTC08), see Table 3.9. In detail in Table 3.9 the letter U sets the direction along the respective axis while R indicates the rotation about the correspondent axis. Sum for every direction and rotation is the progressive sum of the participating mass (PM). Figure 3.14 shows the modal shapes and related dynamic parameters.

| StepNum | Period (secs) | UX | UY | UZ | SumUX | SumUY | SumUZ | RX | RY | RZ | SumRX | SumRY | SumRZ |
|---|---|---|---|---|---|---|---|---|---|---|---|---|---|
| 1 | 0.67 | 0% | 88% | 0% | 0% | 88% | 0% | 99% | 0% | 8% | 99% | 0% | 8% |
| 2 | 0.60 | 89% | 0% | 0% | 89% | 88% | 0% | 0% | 100% | 80% | 99% | 100% | 88% |
| 3 | 0.19 | 0% | 11% | 0% | 89% | 98% | 0% | 0% | 0% | 1% | 99% | 100% | 89% |
| 4 | 0.17 | 10% | 0% | 0% | 99% | 98% | 0% | 0% | 0% | 9% | 99% | 100% | 98% |
| 5 | 0.12 | 0% | 1% | 0% | 99% | 100% | 0% | 0% | 0% | 0% | 99% | 100% | 98% |
| 6 | 0.11 | 1% | 0% | 0% | 100% | 100% | 0% | 0% | 0% | 1% | 99% | 100% | 99% |
| 7 | 0.09 | 0% | 0% | 0% | 100% | 100% | 0% | 0% | 0% | 0% | 99% | 100% | 99% |
| 8 | 0.08 | 0% | 0% | 0% | 100% | 100% | 0% | 0% | 0% | 0% | 99% | 100% | 99% |
| 9 | 0.07 | 0% | 0% | 0% | 100% | 100% | 0% | 0% | 0% | 1% | 99% | 100% | 100% |
| 10 | 0.05 | 0% | 0% | 0% | 100% | 100% | 0% | 0% | 0% | 0% | 99% | 100% | 100% |
| 11 | 0.05 | 0% | 0% | 0% | 100% | 100% | 0% | 0% | 0% | 0% | 99% | 100% | 100% |
| 12 | 0.05 | 0% | 0% | 0% | 100% | 100% | 0% | 0% | 0% | 0% | 99% | 100% | 100% |
| 13 | 0.03 | 0% | 0% | 86% | 100% | 100% | 86% | 1% | 0% | 0% | 100% | 100% | 100% |
| 14 | 0.02 | 0% | 0% | 0% | 100% | 100% | 86% | 0% | 0% | 0% | 100% | 100% | 100% |
| 15 | 0.02 | 0% | 0% | 0% | 100% | 100% | 86% | 0% | 0% | 0% | 100% | 100% | 100% |
| 16 | 0.02 | 0% | 0% | 0% | 100% | 100% | 86% | 0% | 0% | 0% | 100% | 100% | 100% |
| 17 | 0.02 | 0% | 0% | 0% | 100% | 100% | 86% | 0% | 0% | 0% | 100% | 100% | 100% |
| 18 | 0.02 | 0% | 0% | 1% | 100% | 100% | 87% | 0% | 0% | 0% | 100% | 100% | 100% |
| 19 | 0.02 | 0% | 0% | 0% | 100% | 100% | 87% | 0% | 0% | 0% | 100% | 100% | 100% |
| 20 | 0.02 | 0% | 0% | 0% | 100% | 100% | 87% | 0% | 0% | 0% | 100% | 100% | 100% |

Table 3.9 Period of vibration (secs) and participation mass respect to X, Y and Z axes.

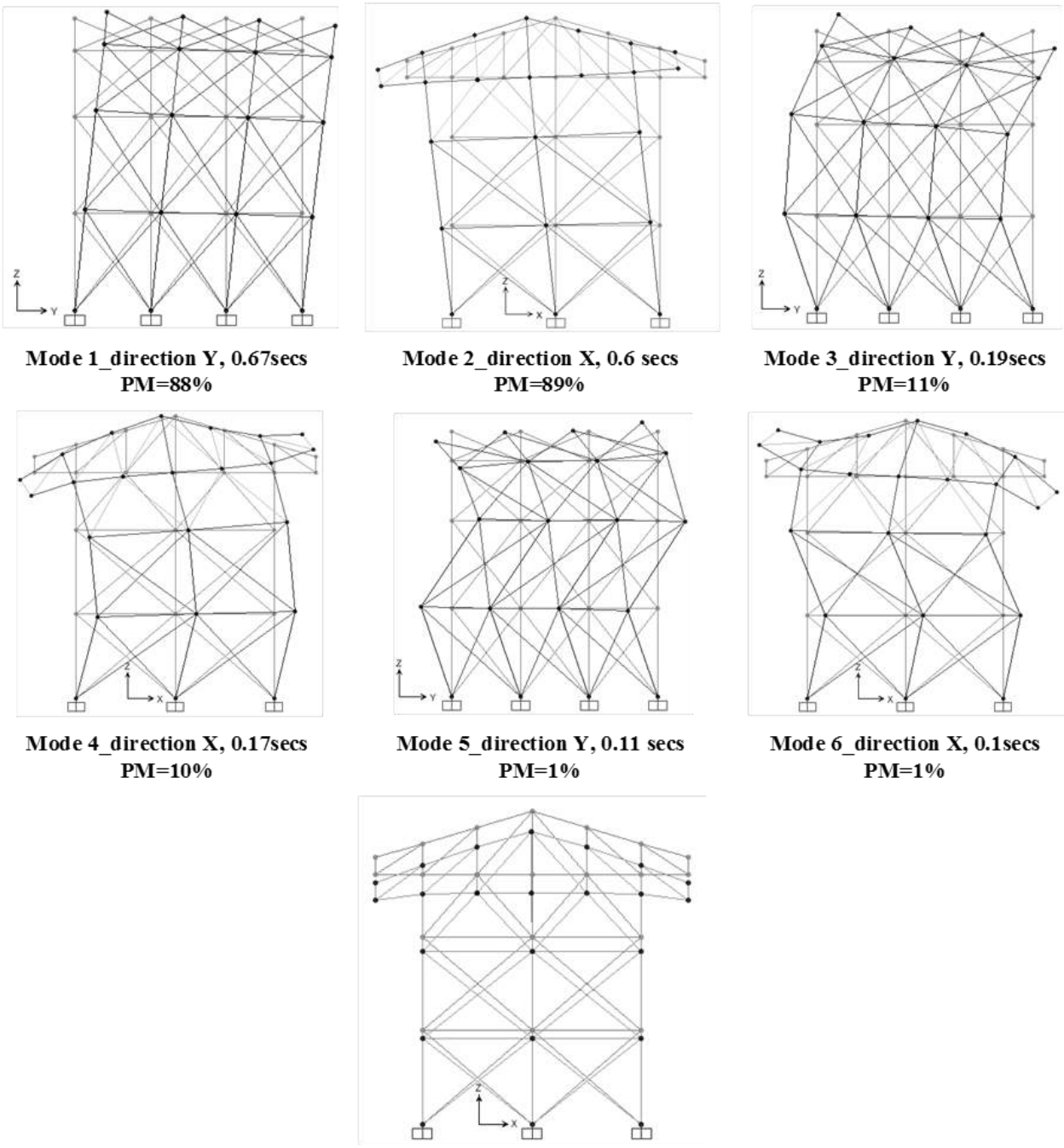


Figure 3.14 Modal analysis, deformed shapes in black color and undeformed shapes in gray color

### 3.4.3.2. **Spectral analysis**

The seismic loading for structural design is realized through response spectra, see Sheet 5, Eurocode 8, 2004 and NTC08, 2008. Design that is in accordance with the requirements of Eurocode 8 has only ULS spectra. Working to the Italian Building Code (NTC08 2008) requires there to be both SLS and ULS spectra.

Based on a 10% probability of exceedance over a reference period of 50 years in the Italian seismic zone 1 (NTC05 2005), and in accordance with Eurocode 8 (2004), the design ground acceleration on type A ground, $a_g$, can be taken to be 0.35$g$. Note that by applying the specific seismic zoning requirements in NTC08 (2008) the designer will have different ground accelerations for the SLS and ULS design response spectra, which are defined to account for the different reference periods of 50 and 712 years. Type A ground is a stiff soil (Eurocode 8, 2004; NTC08, 2008) characterized by rock or other rock-like geological formation, including at most 3 m from using NTC08 (2008) or 5 m from using Eurocode 8 (2004), of weaker material below the surface possessing a shear wave velocity ($v_s$) in excess of > 800 m/s.

### 3.4.3.2.1. **Elastic response spectrum**

The Eurocode 8 spectra are compared with the spectra obtained using the specific design parameters for considered zone, which are taken from the Italian Building Code (NTC08 2008).

For the structure in exam the parameter values listed in Table 3.10 are used to specify this horizontal spectrum (for type A ground conditions) with the damping coefficient $\zeta$ set to 0.05. The parameters from using Eurocode 8 are presented in column (2) and the SLS and ULS parameters from using NTC08 (2008) are given in columns (4) and (5), respectively. Comparing the rows in columns (2) and (5) shows the differences in the parameters for Eqs. (a) to (d) of Sheets 6 and 7 between the two standards. Euroocde 8 seismic loading is more severe than the Italian seismic loading. Parameters for the vertical spectrum are listed in column (3) of Table 3.10 for Eurocode 8 (2004) and in columns (6) and (7) for NTC08 (2008).

| Parameters | Eurocode 8 | | NTC08 | | | |
|---|---|---|---|---|---|---|
| | Components | | | | | |
| | Horizontal | Vertical | Horizontal | | Vertical | |
| | | | SLS | ULS | SLS | ULS |
| (1) | (2) | (3) | (4) | (5) | (6) | (7) |
| $a_g$ (g) | 0.35 | - | 0.125 | 0.3 | - | - |
| $a_{vg}$ (g) | - | 0.9 $a_g$ | - | - | 0.06 | 0.222 |
| $F_h$ | 2.5 | - | 2.316 | 2.384 | - | - |
| $F_v$ | - | 3 | - | - | 1.105 | 1.762 |
| $S$ | 1 | | 1 | 1 | 1 | 1 |
| $\eta$ | 1 | | 1 | 1 | 1 | 1 |
| $T_B$ (s) | 0.15 | 0.05 | 0.097 | 0.119 | 0.05 | |
| $T_C$ (s) | 0.4 | 0.15 | 0.29 | 0.356 | 0.15 | |
| $T_D$ (s) | 2 | 1 | 2.1 | 2.799 | 1 | |

*Note: - is for not applicable.*

Table 3.10 Spectra parameters (Eurocode 8, 2004, NTC08, 2008)

Plotted in Figure 3.15a are the two elastic spectra at SLS for the horizontal $S_e(T)$ and vertical $S_{ve}(T)$ acceleration components for NCT08 and Eurocode 8. Three distinct stages in the seismic response are established by the time parameters $T_B$, $T_C$, and $T_D$ with Eqs. (a) to (d) in Sheets 6 and 7.

### 3.4.3.2.2. **Design spectra for ULS design**

The design seismic action $S_d(T)$ is given by the elastic response spectra with the elastic accelerations (forces) adjusted downward by dividing by $q$, Sheet 8.

One outcome on making this is that, because $\eta = 1/q$, the parameter $\eta$ becomes 0.67 (i.e. damping coefficient $\zeta$ is assumed to be 0.05). With the modelling assumption that $q$ = 1.5, the Eurocode 8 spectra for the horizontal and vertical components remain defined by the four expressions in Sheet 6, respectively, with parameters $F_o$ and $F_v$ reduced by $q$ = 1.5.

Figure 3.15b presents the design spectra for ULS design from Eurocode 8 (2004) and NTC08 (2008), using the same plot construction as in Figure 3.15a and the parameters given in Table 3.10 (see Sheets 6, 7 and 8). It is observed that there has been no change in the Eurocode 8 spectra between Figures 3.15a and 3.15b, while the NCT08 spectra curves of NTC08-horizontal and NTC08-vertical in Figure 3.15b have much higher values than in Figure 3.15a.

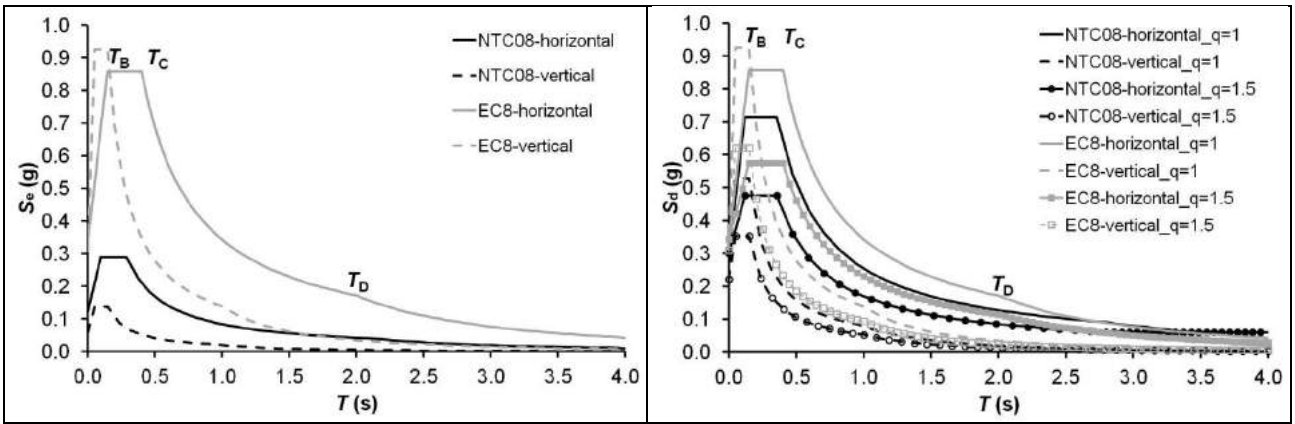


(a) (b)

Figure 3.15 Elastic response spectra in SLS (a) and design response spectra for ULS (b)

### 3.4.3.2.3. **Displacement response spectra**

The displacement response spectra $S_{De}$ through equation of Sheet 6 for the horizontal component (defined by Eqs. (a) to (d) in Sheet 6) gives a direct transformation that is valid for a vibration period $T$, that is not > 4.5 s (4.5 s is time parameter $T_E$ for a type A ground). Plotted in Figure 3.16 is $S_{De}$ using Eq. in Sheet 6 for the Eurocode 8 (EC8-horizontal) and for the NCT08 (NTC08-horizontal).

The elastic displacement response spectrum of horizontal components of seismic actions is extracted by acceleration response of Figure 3.15b. The dashed lines of Figure 3.16 show the displacements calculated with NTC08 and EC8 considering $q$=1. In the same figure the elastic displacement response spectra have been calculated considering $q$=1.5. Figure 3.16 shows that the structure responds to the design seismic action resisting to a maximum displacement of 116mm for EC8 and 124mm for NTC8. Also the effect of the behaviour factor is shown through the reduction of the displacements (see Sheet 8).

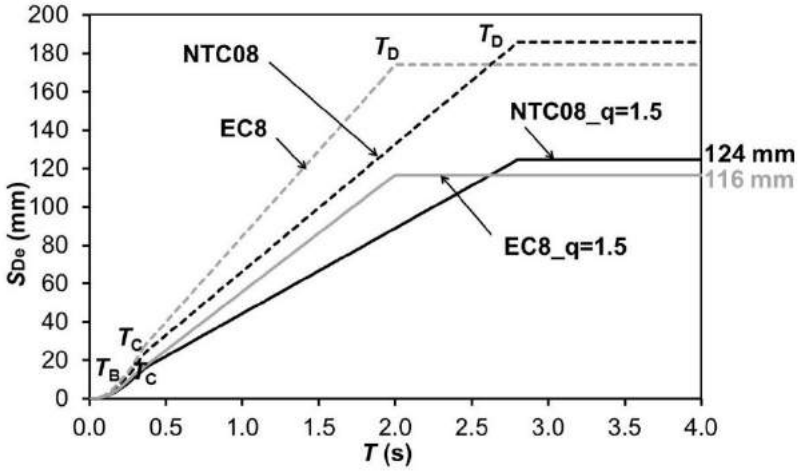


Figure 3.16 Horizontal displacement response spectra

In the seismic combination at ultimate limit state the horizontal (X and Y) and vertical components (Z) that have been considered are NTC08-horizontal_q=1.5 and NTC08-vertical_q=1.5 respectively, of Figure 3.15, through the combinations shown in Table 3.11 (NTC08, §7.3.5 and EN 1998-1-1:2004); the *Z* combination can be ignored if not necessary.

| X direction | Y direction | Z direction |
|---|---|---|
| $1E_x + 0.3E_y + 0.3E_z$ | $0.3E_x + 1E_y + 0.3E_z$ | $0.3E_x + 0.3E_y + 1E_z$ |

Table 3.11 Combination of the horizontal (X and Y) and vertical components (Z)

In the spectral analysis all the vibration modes with a participating mass bigger than 5% should be considered summing up a number of modes so that the total participating mass is larger than 85% (§7.3.3.1 of NTC08). In order to calculate stresses and displacements in the structure, the complete quadratic combination CQC rule may be used.

Through the spectral analysis the maximum displacements in *x* and *y* direction, taking into account the previous combinations, are shown in Figure 3.17 where deformed shapes are in red and undeformed in gray. The assumed limitation of inter-story drift is < 0.01h with h=height of inter-

story (§4.4.3.2 in EC8). For both seismic directions the analysis is satisfied, 42.2 mm < 46 mm (x direction) and 15.9 mm < 46 mm (y direction).

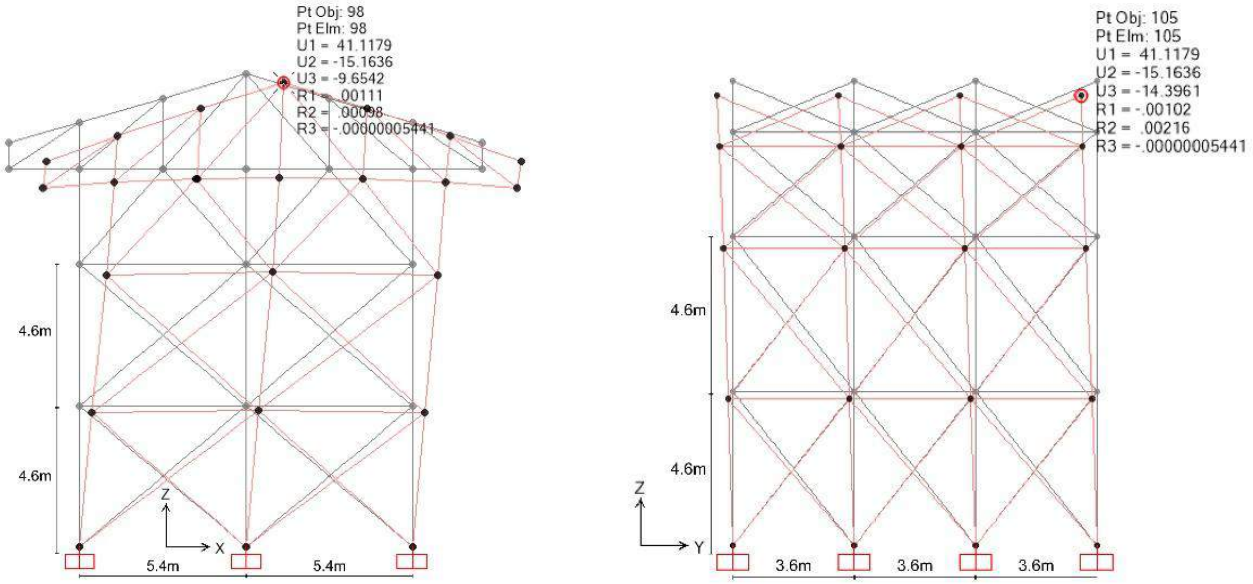


Seismic action in x direction, maximum inter-story drift = 42.2 mm

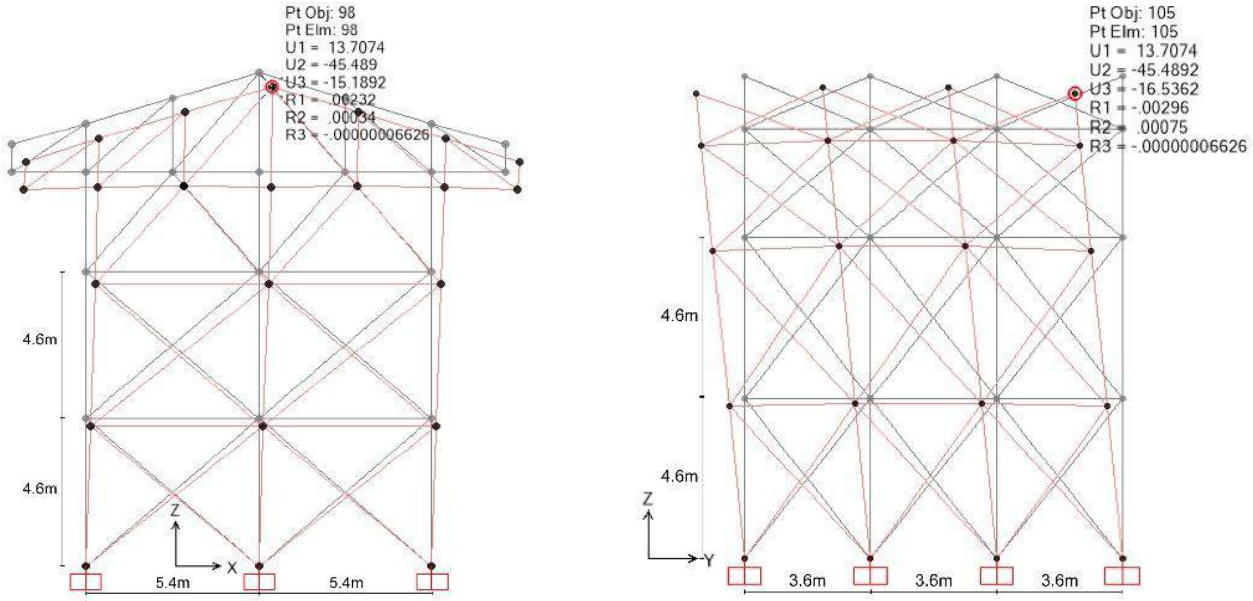


Seismic action in y direction, maximum inter-story drift = 15.9 mm

Figure 3.17 Maximum displacements (Spectral analysis)

### 3.4.3.3. **Pushover analysis**

Two different horizontal actions have been studied as suggested in the chapter §4.3.3.4.2.2 of Eurocode 8:

i) horizontal load proportional to the mass distribution (denoted as ‘‘Mass’’),

ii) horizontal load proportional to the lateral force distribution of the mode with the highest mass participation (denoted as ‘‘Modal’’).

The seismic design codes (EC8 and NTC08) have suggested the use of both configurations. For both analyses the P-Δ effect must be taken into account, see Sheet 8.

As specified by Eurocode 8 (§4.3.3.4.2.3.) the maximum lateral displacement could be between zero and the value corresponding to 150% of the target displacement (defined in §4.3.3.4.2.6. of EC8).

The target displacement has been determined from the elastic response spectrum, see Sheet 7, following the annex B of Eurocode 8 (EN 1998-1:2004).

For the case in exam the modal and mass pushover methods have been addressed as required by specific standards.

Figure 3.18 compares the capacity curves of different methods (a) mass, (b) modal and (c) the Acceleration Displacement Response Spectrum (ADRS) extracted by the modal curve (Figure 3.18b).

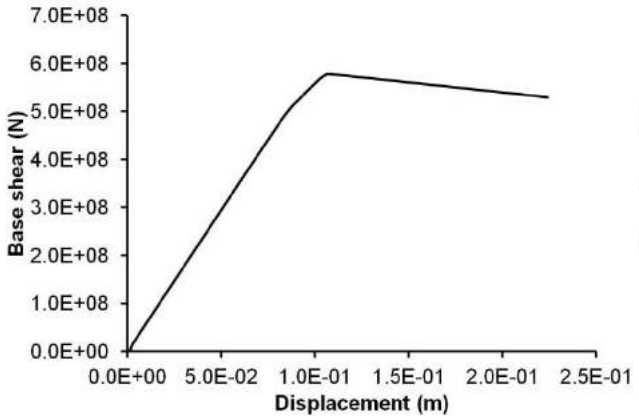


**(a) mass**

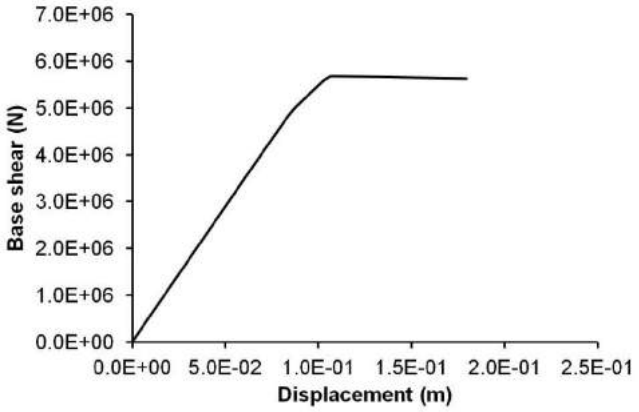


**(b) modal**

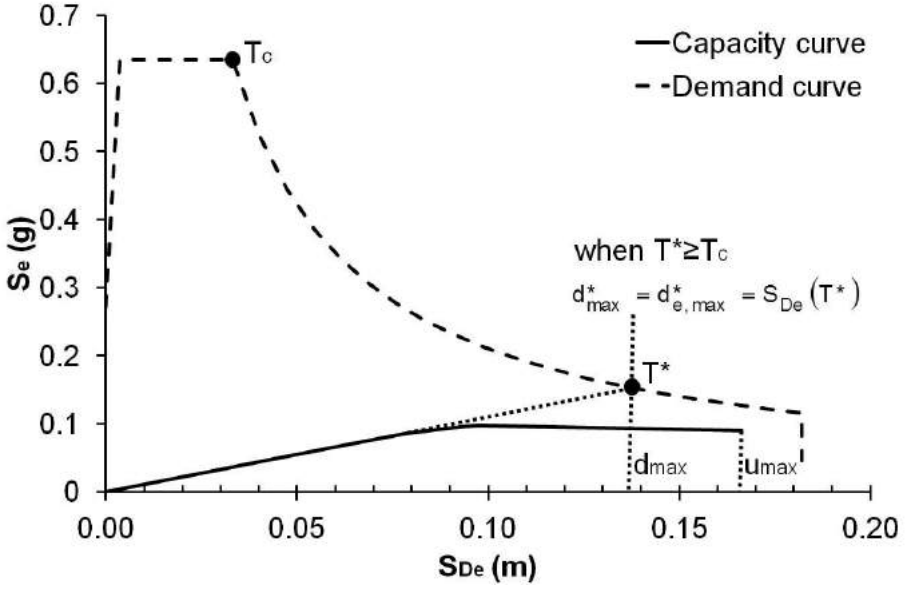


**(c) ADRS of modal curve of (b)**

Figure 3.18 Capacity curves: (a) mass, (b) modal and (c) ADRS of modal curve of (b)

The maximum displacements of capacity curves (Figure 3.18a and b), equal to 224 mm and 179 mm for mass and modal methods respectively, show that the displacement capacity of the structure in exam is greater than the required displacement capacity determined for that site (116 mm), see curve EC8_q=1.5 of Figure 3.16. For this reason the seismic analysis of the structure is satisfied.

The demand curve (detailed in Sheet 7) is used in agreement with the capacity curve to predict the target displacement point *T**, see Figure 3.18c.

Considering the case in exam, $u_{max}$ = 0.179m and $d_{max}$ = 0.1375 m, see Figure 3.18c, the seismic analysis is verified.

## 3.5. **ULS analysis**

In the following the diagrams of the forces and moments in four frames are reported for the different ultimate limit state load combinations, and an example of structural verification of a compressed member is carried out. The diagrams relative to the seismic load combinations present two values of the internal actions in the frame elements, since the oscillations due to the earthquake produce internal actions with opposite signs. Only the diagrams in the *x*-*z* plane are considered, for which the highest values of forces and moments are obtained. The structural verification is based on the formulations given in (CNR-DT205/2007). Anyway, since in the document mentioned above only double-T sections are considered, indications are given also for the verification of other kinds of profiles, on the base of formulations available in the literature (Bank 2006, Kollar 2003, Tarjan et al 2010a-b).

### 3.5.1. **Forces and moments diagrams**

In the following every figure shows the forces and moment diagrams of the structure subjected to the different load combinations in x- and y-direction, see Table 3.4. In every scheme the most stressed member is evidenced by a black circle and the related value of the internal action is indicated for the specific frame detailed in Figure 3.1.

#### 3.5.1.1. **Axial force**

| | | | | |
|---|---|---|---|---|
| 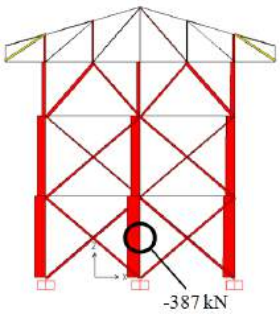 | Frame 1 = -387kN | Frame 2 = -467kN | Frame 3 = -467kN | Frame 4 = -387kN |
| Wind in x-direction | | | | |
| 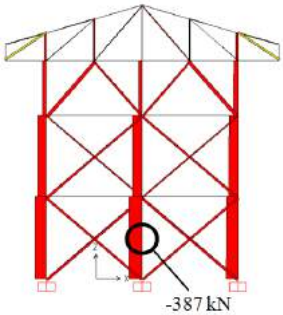 | Frame 1 = -387kN | Frame 2 = -467kN | Frame 3 = -467kN | Frame 4 = -387kN |
| Wind in y-direction | | | | |

Figure 3.19 Fundamental load combination, axial force diagrams

| | | | | | | |
|---|---|---|---|---|---|---|
| 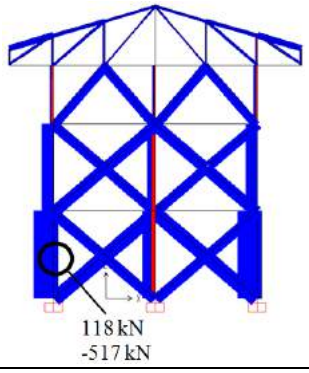 | Frame 1 | 118kN<br>-517kN | Frame 2 | 49kN<br>-510kN | Frame 3 | 49kN<br>-510kN | Frame 4 | 118kN<br>-517kN |
| Earthquake in x-direction | | | | | | | | |
| 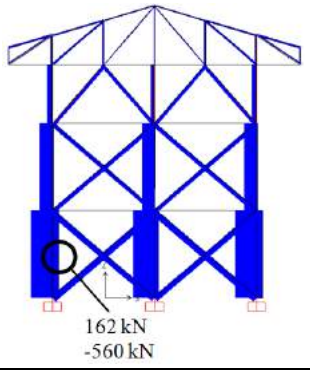 | Frame 1 | 162kN<br>-560kN | Frame 2 | -114kN<br>-348kN | Frame 3 | -114kN<br>-348kN | Frame 4 | 162kN<br>-560kN |
| Earthquake in y-direction | | | | | | | | |

Figure 3.20 Seismic load combination, axial force diagrams

#### 3.5.1.2. **Bending moment**

| | | | | | | |
|---|---|---|---|---|---|---|
| 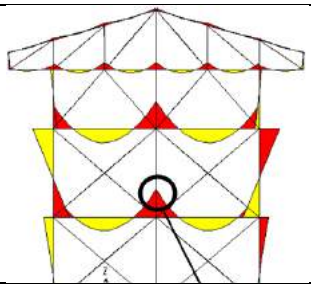 | Frame 1 | 71922 kNmm | Frame 2 | 134739 kNmm | Frame 3 | 134739 kNmm |
| 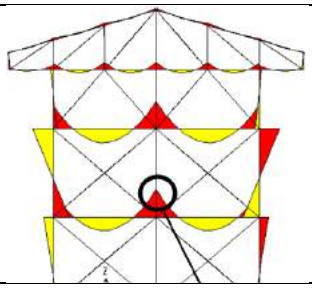 | Frame 1 | 71922 kNmm | Frame 2 | 134739 kNmm | Frame 3 | 134739 kNmm |

| | | | | | |
|---|---|---|---|---|---|
| | Frame 4 | 71922 kNmm | | Frame 4 | 71922 kNmm |
| Wind in x-direction | | | Wind in y-direction | | |

Figure 3.21 Fundamental load combination, bending moment diagrams

| | | | | | |
|---|---|---|---|---|---|
| 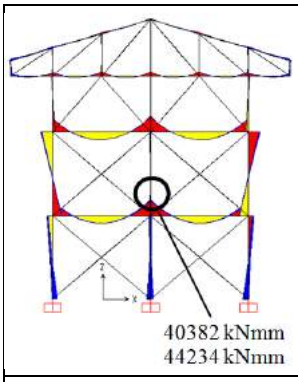 | Frame 1 | 40382kNmm<br>44234kNmm | 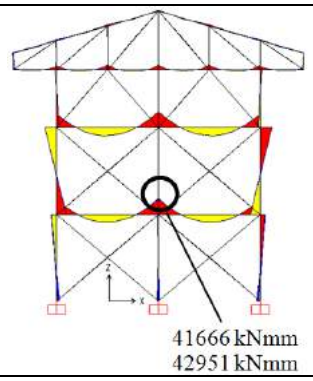 | Frame 1 | 41666kNmm<br>42951kNmm |
| | Frame 2 | 76312kNmm<br>80221kNmm | | Frame 2 | 77615kNmm<br>78918kNmm |
| | Frame 3 | 76312kNmm<br>80221kNmm | | Frame 3 | 76312kNmm<br>80221kNmm |
| | Frame 4 | 40384kNmm<br>44236kNmm | | Frame 4 | 41667kNmm<br>42952kNmm |
| Earthquake in x-direction | | | Earthquake in y-direction | | |

Figure 3.22 Seismic load combination, bending moment diagrams

3.5.1.3. **Shear force**

| | | | |
|---|---|---|---|
| 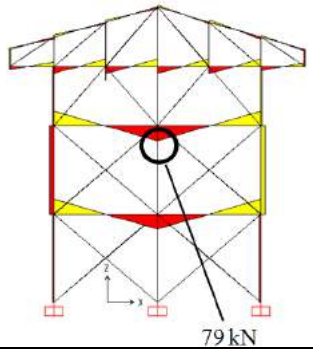 | Frame 1 = 79kN | 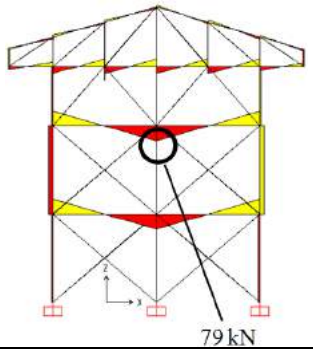 | Frame 1 = 79kN |
| | Frame 2 = 149kN | | Frame 2 = 149kN |
| | Frame 3 = 149kN | | Frame 3 = 149kN |
| | Frame 4 = 79kN | | Frame 4 = 79kN |
| Wind in x-direction | | Wind in y-direction | |

Figure 3.23 Fundamental load combination, shear force diagrams

| | | | | | |
|---|---|---|---|---|---|
| 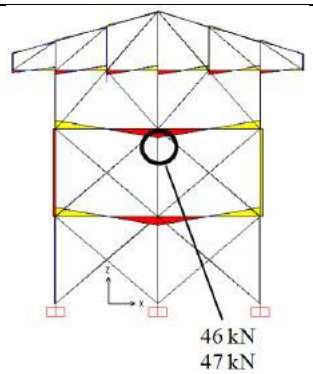 | Frame 1 | 46kN<br>47kN | 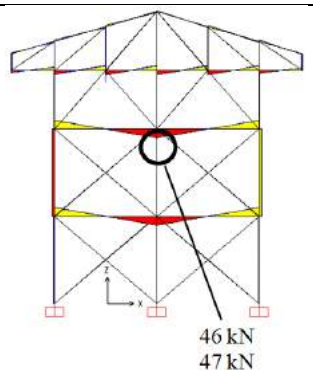 | Frame 1 | 46kN<br>47kN |
| | Frame 2 | 86kN<br>87kN | | Frame 2 | 87kN<br>87kN |
| | Frame 3 | 86kN<br>87kN | | Frame 3 | 87kN<br>87kN |
| | Frame 4 | 46kN<br>47kN | | Frame 4 | 46kN<br>47kN |
| Earthquake in x-direction | | | Earthquake in y-direction | | |

Figure 3.24 Seismic load combination, shear force diagrams

### 3.5.1.4. **Torsional moment**

| | | | |
|---|---|---|---|
| 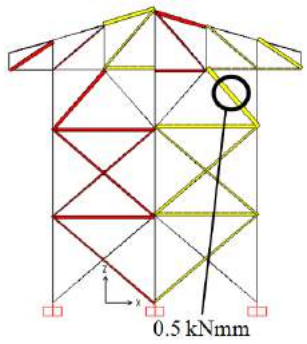 | Frame 1 = 0.5kNmm | 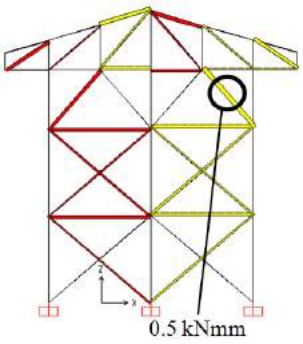 | Frame 1 = 0.5kNmm |
| | Frame 2 = 0.02kNmm | | Frame 2 = 0.02kNmm |
| | Frame 3 = 0.03kNmm | | Frame 3 = 0.03kNmm |
| | Frame 4 = 0.5kNmm | | Frame 4 = 0.5kNmm |
| Wind in x-direction | | Wind in y-direction | |

Figure 3.25 Fundamental load combination, torsional moment diagrams

| | | | | | |
|---|---|---|---|---|---|
| 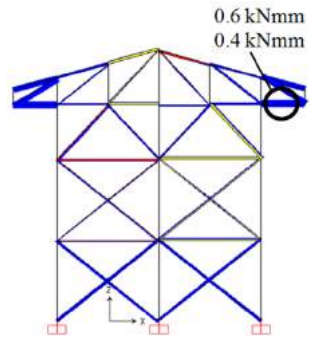 | Frame 1 | 0.6kNmm<br>0.4kNmm | 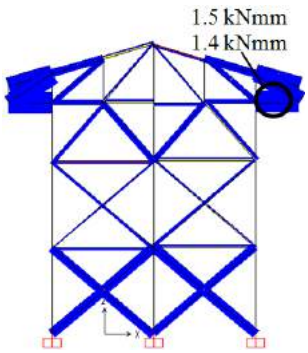 | Frame 1 | 1.5kNmm<br>1.4kNmm |
| | Frame 2 | 0.5kNmm<br>0.4kNmm | | Frame 2 | 1.5kNmm<br>1.4kNmm |
| | Frame 3 | 0.5kNmm<br>0.4kNmm | | Frame 3 | 1.5kNmm<br>1.4kNmm |
| | Frame 4 | 0.6kNmm<br>0.4kNmm | | Frame 4 | 0.6kNmm<br>0.4kNmm |
| Earthquake in x-direction | | | Earthquake in y-direction | | |

Figure 3.26 Seismic load combination, torsional moment diagrams

### 3.5.2. **Example of verification of a compressed member**

The next verifications – in detail till page 84 – will be proposed., as anticipated in the introduction, strictly following the CNR-DT205/2007 and the more recent CEN TC250 WG4L (2016). As an example, a buckling verification is carried out for the member in compression evidenced in Figure 3.27. The stability verification of a compressed member requires the following relation to be satisfied:

$$N_{c,Sd} \leq N_{c,Rd2} \qquad (3.4)$$

where $N_{c,Rd2}$ is the design value of force that causes buckling of the member.

| | | |
|---|---|---|
| 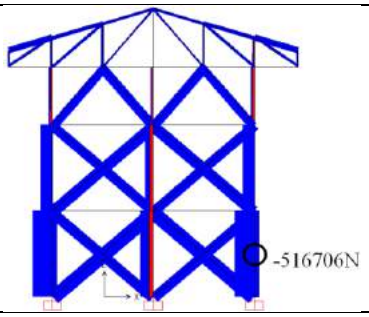  | Frame 4 | -516706 N |
| Earthquake in x-direction | | |

Figure 3.27 Seismic load combination, axial force diagram

In order to carry out the stability verification, the built-up cross-section of the member (2 U 300x100x15 mm) is considered as being a 300x200 double-T section, with the thickness of the web equal to 30 mm and the thickness of the flanges equal to 15 mm.

For the case of double-T profiles the value of $N_{c,Rd2}$ is computed as:

$$N_{c,Rd\,2} = k \cdot N_{loc,Rd} \tag{3.5}$$

where the design value of the compression force that causes the local instability of the profile, $N_{loc,Rd}$, can be deduced from the relation:

$$N_{loc,Rd} = A \cdot f_{loc,d}^{axial} \tag{3.6}$$

where $f_{loc,d}^{axial}$ is the design value of the local critical stress, and can be computed as:

$$f_{loc,d}^{axial} = \frac{1}{\gamma_f} \cdot \min\left\{\left(f_{loc,k}^{axial}\right)_f, \left(f_{loc,k}^{axial}\right)_w\right\} \tag{3.7}$$

where $\left(f_{loc,k}^{axial}\right)_f$ and $\left(f_{loc,k}^{axial}\right)_w$ represent, respectively, the critical stress of the flanges and of the web.

For the ultimate limit states, the partial coefficient of the material, $\gamma_f$, can be obtained by the expression:

$$\gamma_f = \gamma_{f1} \cdot \gamma_{f2} \tag{3.8}$$

where factor $\gamma_{f1}$ takes into account the uncertainty level in the determination of the material properties with a coefficient of variation $V_x$ (Table 3.12); factor $\gamma_{f2}$ takes into account the brittle behaviour of the material and for it a value of 1.30 is suggested by CNR-DT205/2007.

| $V_x \leq 0.10$ | $0.10 < V_x \leq 0.20$ |
|---|---|
| 1.10 | 1.15 |

Table 3.12 Values of the coefficient of variation $V_x$

The value of the coefficient of variation $V_x$ related to the characteristic strength or deformation property of the material must be determined through an appropriate series of experimental tests.

For the serviceability limit states the unit value is suggested for the material partial coefficient.

Adopting the symbols of Figure 3.28, the value of $\left(f_{loc,k}^{axial}\right)_f$ can be conservatively assumed equal to:

$$\left(f_{loc,k}^{axial}\right)_f = 4 \cdot G_L \cdot \left(\frac{t_f}{b_f}\right)^2 \tag{3.9}$$

where $G_L$ is the shear modulus. The use of equation (3.9) corresponds to considering the flanges as simply supported in correspondence of the web. In order to consider the restraint degree offered by the web it is suggested to adopt the formulations reported in Appendix A of (CNR-DT205/2007).

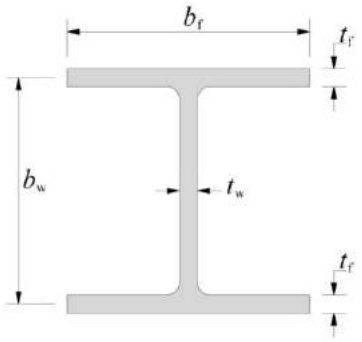


Figure 3.28 Double-T section: symbols adopted for the geometrical properties (CNR-DT205/2007)

Similarly, the value of the critical stress in the compressed web, $\left(f_{loc,k}^{axial}\right)_w$, can conservatively be assumed equal to (CNR-DT205/2007):

$$\left(f_{loc,k}^{axial}\right)_w = k_c \cdot \frac{\pi^2 \cdot E_{Lc} \cdot t_w^2}{12 \cdot \left(1 - \nu_L \cdot \nu_T\right) \cdot b_w^2} \tag{3.10}$$

where $E_{Lc}$ is the longitudinal compressive elastic modulus, $v_L$ is the longitudinal Poisson ratio and $v_T$ is the transverse Poisson ratio.

Coefficient $k_c$ is given by:

$$k_c = 2 \cdot \sqrt{\frac{E_{Tc}}{E_{Lc}}} + 4 \cdot \frac{G}{E_{Lc}} \cdot \left(1 - v_L^2 \cdot \frac{E_{Tc}}{E_{Lc}}\right) + 2 \cdot v_L \cdot \frac{E_{Tc}}{E_{Lc}} \tag{3.11}$$

where $E_{Tc}$ is the transverse compressive elastic modulus, $E_{Lc}$ is the longitudinal compressive elastic modulus, $G_L$ is the shear modulus, $v_L$ is the longitudinal Poisson.

Coefficient $k$ of equation (3.5) represents a reduction factor that takes into account the interaction between local and global buckling of the member. This coefficient assumes a unit value if the slenderness of the member tends to zero or in presence of restraints that prevent global buckling. The value of the coefficient can be computed as (CNR-DT205/2007):

$$k = \frac{1}{c \cdot \lambda^2} \cdot \left(\Phi - \sqrt{\Phi^2 - c \cdot \lambda^2}\right) \tag{3.12}$$

where symbol $c$ denotes a numerical coefficient that, in absence of more accurate experimental evaluations, can be assumed equal to 0.65, and:

$$\Phi = \frac{1 + \lambda^2}{2} \tag{3.13}$$

The slenderness $\lambda$ is equal to:

$$\lambda = \sqrt{\frac{N_{loc,Rd}}{N_{Eul}}} \tag{3.14}$$

with:

$$N_{Eul} = \frac{1}{\gamma_f} \cdot \frac{\pi^2 \cdot E_{eff} \cdot I_{\min}}{L_0^2} \tag{3.15}$$

In equation (3.15) $E_{eff}$ is the effective modulus of elasticity, $I_{min}$ is the minimum moment of inertia of the cross-section and $L_0$ is the effective length of the member.

In Figure 3.29a the trend of $k$ for varying $\lambda$ is represented.

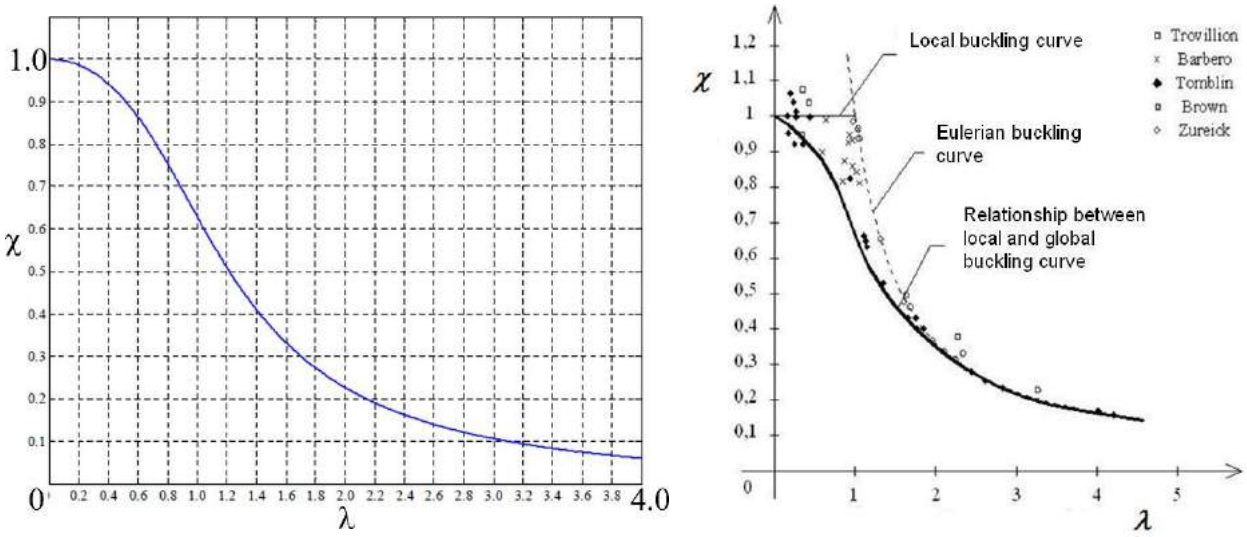


(a) (b)

Figure 3.29 Local and global buckling modes for columns: (a) CNR-DT205/2007 and (b) Barbero, 1999.

The effective length of the member, $L_0$, to be introduced in equation (3.15), can be evaluated through the formulations reported in Eurocode 3. For a column in a non-sway mode, as for the case in exam, the buckling length ratio $l/L$ can be obtained from the diagram of Figure 3.30.

For a continuous column, as the one in exam, and with reference to Figure 3.31, coefficients $\eta_1$ and $\eta_2$ can be obtained from relations (Eurocode 3):

$$\eta_1 = \frac{K_c + K_1}{K_c + K_1 + K_{11} + K_{12}} \tag{3.16}$$

$$\eta_2 = \frac{K_c + K_2}{K_c + K_2 + K_{21} + K_{22}} \tag{3.17}$$

where $K_c$ is the stiffness coefficient of the column $I/L$ ($I$ = second moment of inertia while $L$ = length of column), $K_1$ and $K_2$ are the stiffness coefficients for the adjacent lengths of columns and $K_{ij}$ is the effective beam stiffness coefficient.

If the beams are not subjected to axial forces, as in the case in exam, their effective stiffness coefficients can be determined from Table 3.13.

| Conditions of rotational restraint at far end of beam | Effective beam stiffness coefficient *K* |
|---|---|
| Fixed at far end | 1.0 *I/L* |
| Pinned at far end | 0.75 *I/L* |
| Rotation as at near end (double curvature) | 1.5 *I/L* |
| Rotation equal and opposite to that at near end (single curvature) | 0.5 *I/L* |
| General case. Rotation $\theta_a$ at near end and $\theta_b$ at far end | $(1 + 0.5\theta_b/\theta_a)$ *I/L* |

Table 3.13 Effective beam stiffness coefficient (Eurocode 3)

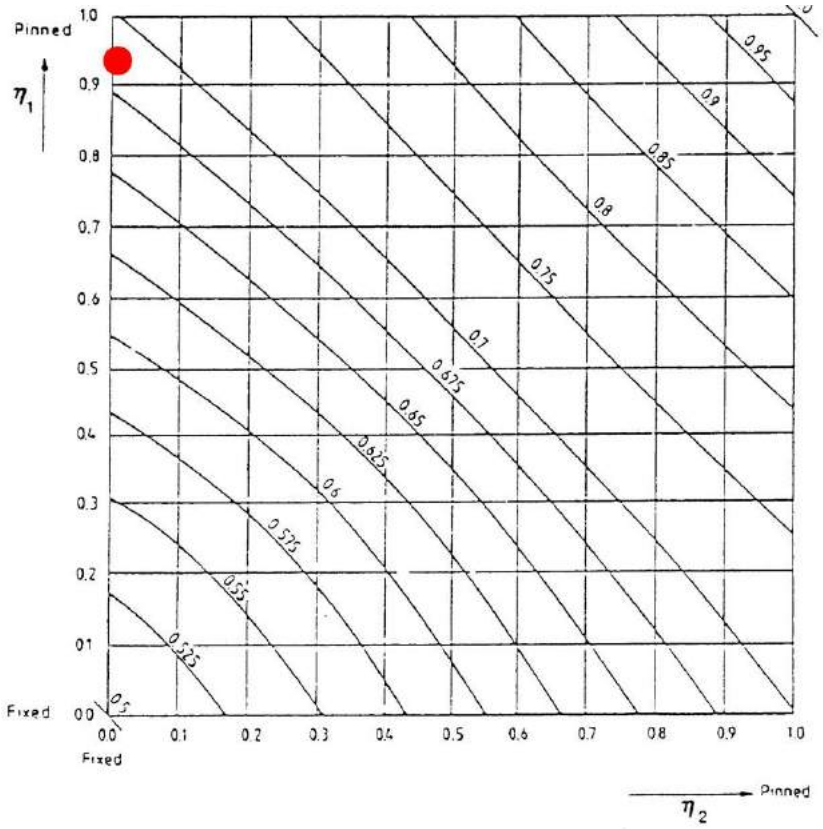


Figure 3.30 Buckling length ratio *l/L* for a column in a non-sway mode (EC3)

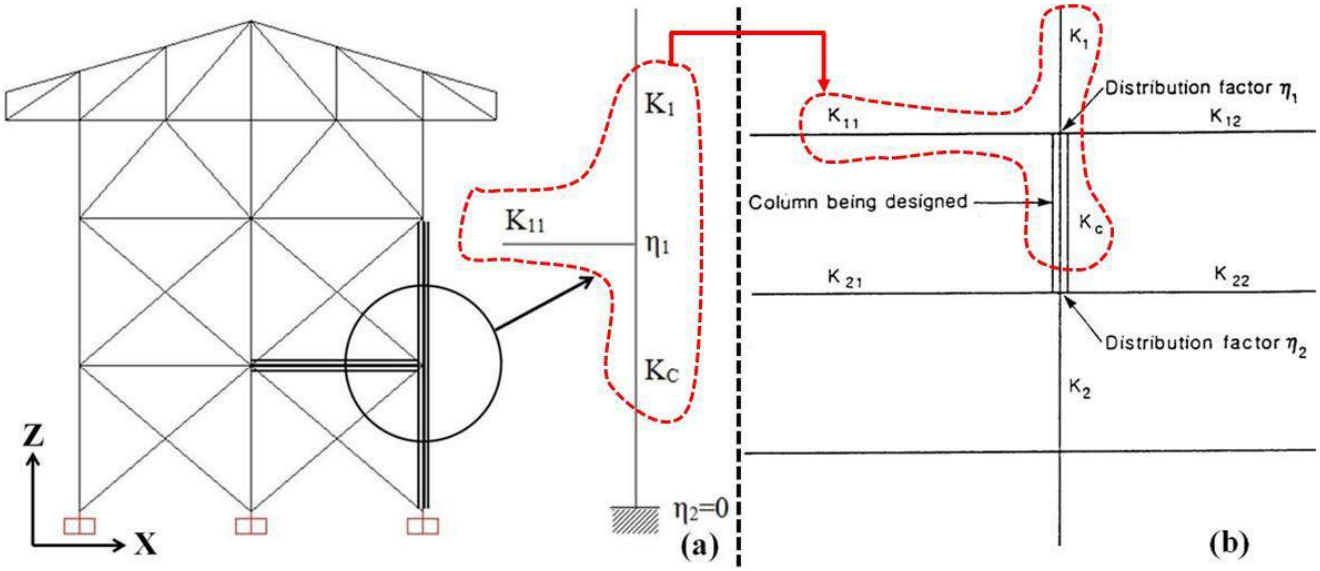


Figure 3.31 Distribution factors for the case in exam (a); distribution factors for continuous columns, EC3 (b)

For the case in exam we have (Figure 3.31a):

$K_c = K_1 = 26811875 / 4600 = 5829 \text{ mm}^3$

$K_{11} = 1.0 \cdot 4687500 / 5400 = 868 \text{ mm}^3$ (fixed at far end, Table 3.13)

$\eta_2 = 0 \text{ mm}^3$ (the base of the column is fixed)

From equation (3.16) we have:

$$\eta_1 = \frac{5829 + 5829}{5829 + 5829 + 868} = 0.93$$

From Figure 3.30, considering $\eta_1$=0.93 and $\eta_2$=0 (see red point in Figure 3.30), a buckling length l/L between 0.675 and 0.7 is obtained. We conservatively adopt the value 0.7. Thus, the effective length of the member, to be introduced in equation (3.15), results:

$L_0 = 4600 \cdot 0.7 = 3220 \text{ mm}$

From equation (3.15) the Euler buckling load results:

$$N_{Eul} = \frac{1}{(1.15 \cdot 1.3)} \cdot \frac{\pi^2 \cdot 23000 \cdot 26811875}{3220^2} = 392249 \text{ N}$$

From equation (3.11) the value of coefficient $k_c$ results:

$$k_c = 2 \cdot \sqrt{\frac{7000}{23000}} + 4 \cdot \frac{4500}{23000} \cdot \left(1 - 0.3^2 \cdot \frac{7000}{23000}\right) + 2 \cdot 0.3 \cdot \frac{7000}{23000} = 2.05$$

From equation (3.10) the value of the critical stress in the compressed web results:

$$\left(f_{loc,k}^{axial}\right)_w = 2.05 \cdot \frac{\pi^2 \cdot 23000 \cdot 30^2}{12 \cdot (1 - 0.3 \cdot 0.3) \cdot 285^2} = 472 \text{ MPa}$$

From equation (3.9) the value of the critical stress of the flanges results:

$$\left(f_{loc,k}^{axial}\right)_f = 4 \cdot 4500 \cdot \left(\frac{15}{200}\right)^2 = 101 \text{ MPa}$$

The design value of the local critical stress, computed through equation (3.7), results:

$$f_{loc,d}^{axial} = \frac{1}{(1.15 \cdot 1.3)} \cdot \min\{101\ ,\ 472\} = 68 \text{ MPa}$$

From equation (3.6) the design value of the compression force that causes the local instability results:

$$N_{loc,Rd} = 14100 \cdot 68 = 958800 \text{ N}$$

From equation (3.14) the slenderness results:

$$\lambda = \sqrt{\frac{958800}{392249}} = 1.56$$

From equation (3.13) we have:

$$\Phi = \frac{1+1.56^2}{2} = 1.72$$

From equation (3.12) coefficient *k* results:

$$k = \frac{1}{0.65 \cdot 1.56^2} \cdot \left(1.72 - \sqrt{1.72^2 - 0.65 \cdot 1.56^2}\right) = 0.35$$

From equation (3.5) the value of $N_{c,Rd2}$ results:

$$N_{c,Rd2} = 0.35 \cdot 958800 = 335580 \text{ N}$$

Since 516706 N > 335580 N the verification is not satisfied. It would be necessary to adopt a stiffer profile for the member. For example, adopting a 400x400x20 mm wide flange profile the critical load would result about 590 kN (using the same value of the effective length) and the verification would result verified.

The reported formulas are valid for the case of a double-T profile. For general cross-section types, the value of $N_{c,Rd2}$ can be assumed.

$$N_{c,Rd2} = \min\left\{N_{c,Rd2,glob}, \frac{1}{\gamma_f} \cdot N_{c,Rd2,loc}\right\} \tag{3.18}$$

where $N_{c,Rd2,glob}$ is the design value of the global buckling strength and $N_{c,Rd2,loc}$ is the design value of the local buckling strength.

The design value of the global buckling strength, $N_{c,Rd2,glob}$, can be computed as following (Bank 2006):

$$N_{c,Rd2,glob} = \frac{N_{Eul}}{1+\left(\frac{N_{Eul}}{G_L \cdot A_V}\right)}$$

where $N_{Eul}$ is the Euler buckling load, defined in equation (3.15), $G_L$ is the design value of the shear modulus and $A_V$ is the shear area of the cross-section.

For box-section profiles, if the webs and the flanges are considered as simply supported, their buckling loads for unit length is (Kollar 2003, Tarjan et al 2010a-b):

$$\left(N_{x,cr}\right)_f^{SS} = \frac{\pi^2}{b_f^2} \cdot \left\{2 \cdot \sqrt{\left(D_{11}\right)_f \cdot \left(D_{22}\right)_f} + 2 \cdot \left[\left(D_{12}\right)_f + 2 \cdot \left(D_{66}\right)_f\right]\right\} \tag{3.19}$$

$$\left(N_{x,cr}\right)_w^{SS} = \frac{\pi^2}{b_w^2} \cdot \left\{2 \cdot \sqrt{\left(D_{11}\right)_w \cdot \left(D_{22}\right)_w} + 2 \cdot \left[\left(D_{12}\right)_w + 2 \cdot \left(D_{66}\right)_w\right]\right\} \tag{3.20}$$

In previous equations (3.19) and (3.20) subscripts *f* and *w* refer to the flange and to the web, respectively, $b$ is the width (see Figure 3.32) and $D_{11}$, $D_{22}$, $D_{12}$ and $D_{66}$ are elements of the bending stiffness matrix $[D]$ of a plate. For a plate consisting of a single orthotropic layer they are given by $D_{11} = \frac{E_1 \cdot h^3}{12 \cdot R}$, $D_{22} = \frac{E_2 \cdot h^3}{12 \cdot R}$, $D_{12} = \nu_{12} \cdot D_{22}$, $D_{66} = \frac{G_{12} \cdot h^3}{12}$

where $R = 1 - \nu_{12}^2 \cdot E_2 / E_1$, $h$ is the thickness of the plate, $\nu_{12}$ is the Poisson's ratio, $E_1$ and $E_2$ are the Young's moduli and $G_{12}$ is the shear modulus.

The flange buckles first when (Kollar 2003, Tarjan et al 2010a-b):

$$\left(N_{x,cr}\right)_f^{SS} \cdot \left(\alpha_{11}\right)_f < \left(N_{x,cr}\right)_w^{SS} \cdot \left(\alpha_{11}\right)_w \tag{3.21}$$

where $\alpha_{11}$ is the tensile compliance of plate. For a plate consisting of a single orthotropic layer:

$$\alpha_{11} = 1/(E_1 \cdot h) \tag{3.22}$$

In this case the webs elastically restrain the rotation of the flange as springs with constant given from (Kollar 2003, Tarjan et al 2010a-b):

$$k = \frac{c \cdot (D_{22})_w}{b_w} \cdot \left( 1 - \frac{(N_{x,cr})_f^{SS} \cdot (\alpha_{11})_f}{(N_{x,cr})_w^{SS} \cdot (\alpha_{11})_w} \right) \tag{3.23}$$

with $c = 2$.

The buckling load for unit length of the flange is then calculated with this spring constant using the following expression:

$$(N_{x,cr})_f = \pi^2 \cdot \left( 2 \cdot \sqrt{1 + 4.139 \cdot \xi} \cdot \sqrt{D_{11} \cdot D_{22}} + \left( 2 + 0.62 \cdot \xi^2 \right) \cdot (D_{12} + 2 \cdot D_{66}) \right) / L_y^2 \tag{3.24}$$

where $L_y$ is the width of the flange, $\xi = 1/(1 + 10\zeta)$ and $\zeta = D_{22} / (k \cdot L_y)$.

The web buckles first when:

$$(N_{x,cr})_f^{SS} \cdot (\alpha_{11})_f > (N_{x,cr})_w^{SS} \cdot (\alpha_{11})_w \tag{3.25}$$

In this case the flanges restrain the rotation of the web, and the spring constant is (Kollar 2003, Tarjan et al 2010a-b):

$$k = \frac{c \cdot (D_{22})_f}{b_f} \cdot \left( 1 - \frac{(N_{x,cr})_w^{SS} \cdot (\alpha_{11})_w}{(N_{x,cr})_f^{SS} \cdot (\alpha_{11})_f} \right) \tag{3.26}$$

with $c = 2$.

The buckling load of the web is calculated with this spring constant by expression (3.27).

For C and Z-section profiles the local buckling loads of the flange, $(N_{x,cr})_f^{SS}$, and of the web, $(N_{x,cr})_w^{SS}$ considered as simply supported, are computed as (Kollar 2003, Tarjan et al 2010a-b):

$$\left(N_{x,cr}\right)_f^{SS} = \frac{12 \cdot \left(D_{66}\right)_f}{b_f^2} \tag{3.27}$$

$$\left(N_{x,cr}\right)_w^{SS} = \frac{\pi^2}{b_w^2} \cdot \left\{2 \cdot \sqrt{\left(D_{11}\right)_w \cdot \left(D_{22}\right)_w} + 2 \cdot \left[\left(D_{12}\right)_w + 2 \cdot \left(D_{66}\right)_w\right]\right\} \tag{3.28}$$

The flange buckles first when:

$$\left(N_{x,cr}\right)_f^{SS} \cdot \left(\alpha_{11}\right)_f < \left(N_{x,cr}\right)_w^{SS} \cdot \left(\alpha_{11}\right)_w \tag{3.29}$$

In this case the web restrains the rotation of the flange (see Figure 3.32), and the spring constant is given from equation (3.26), with $c = 2$ .

The buckling load of the flanges is calculated with this spring constant by the following expressions:

$$\left(N_{x,cr}\right)_f = \sqrt{D_{11} \cdot D_{22}} \cdot \begin{pmatrix} K\left(\eta \cdot 15.1 \cdot \sqrt{1-\nu} + \left(1-\eta\right) \cdot 6 \cdot \left(1-\nu\right)\right) + \\ + 7 \cdot \left(1-K\right) / \sqrt{1 + 4.12 \cdot \zeta} \end{pmatrix} / L_y^2 \qquad \text{when} \quad K \le 1 \tag{3.30}$$

$$\left(N_{x,cr}\right)_f = \sqrt{D_{11} \cdot D_{22}} \cdot \left(\eta \cdot 15.1 \cdot \sqrt{1-\nu} + \left(K-\eta\right) \cdot 6 \cdot \left(1-\nu\right)\right) / L_y^2 \qquad \text{when} \quad K > 1 \tag{3.31}$$

Where $K = \left(2 \cdot D_{66} + D_{12}\right) / \sqrt{D_{11} \cdot D_{22}}$ , $\eta = 1 / \sqrt{1 + \left(7.22 - 3.55 \cdot \nu\right) \cdot \zeta}$ and $\nu = D_{12} / \left(2 \cdot D_{66} + D_{12}\right)$ .

The web buckles first when:

$$\left(N_{x,cr}\right)_f^{SS} \cdot \left(\alpha_{11}\right)_f > \left(N_{x,cr}\right)_w^{SS} \cdot \left(\alpha_{11}\right)_w \tag{3.32}$$

In this case the flanges restrain the rotation of the edges of the web and the restraining torsional stiffness is given as indicated in equation 3.33 (see Figure 3.32):

$$G_L \cdot J_t = 4 \cdot \left(D_{66}\right)_f \cdot b_f \cdot \left(1 - \frac{\left(N_{x,cr}\right)_w^{SS} \cdot \left(\alpha_{11}\right)_w}{\left(N_{x,cr}\right)_f^{SS} \cdot \left(\alpha_{11}\right)_f}\right) \tag{3.33}$$

The buckling load is then calculated by expression (3.27).

For L-section profiles the local buckling loads of the flange, $\left(N_{x,cr}\right)_f^{SS}$, and of the web, $\left(N_{x,cr}\right)_w^{SS}$, considered as simply supported, are computed as (Kollar 2003, Tarjan et al 2010a-b):

$$\left(N_{x,cr}\right)_f^{SS} = \frac{12 \cdot \left(D_{66}\right)_f}{b_f^2} \tag{3.34}$$

$$\left(N_{x,cr}\right)_w^{SS} = \frac{12 \cdot \left(D_{66}\right)_w}{b_w^2} \tag{3.35}$$

The flange buckles first when:

$$\left(N_{x,cr}\right)_f^{SS} \cdot \left(\alpha_{11}\right)_f < \left(N_{x,cr}\right)_w^{SS} \cdot \left(\alpha_{11}\right)_w \tag{3.36}$$

In this case the web restrains the rotation of the flanges (see Figure 3.32), and the restraining torsional stiffness is given from:

$$G_L \cdot J_t = 4 \cdot \left(D_{66}\right)_w \cdot b_w \cdot \left(1 - \frac{\left(N_{x,cr}\right)_f^{SS} \cdot \left(\alpha_{11}\right)_f}{\left(N_{x,cr}\right)_w^{SS} \cdot \left(\alpha_{11}\right)_w}\right) \tag{3.37}$$

The buckling load of the flange is calculated with this torsional stiffness by the following expression:

$$\left(N_{x,cr}\right)_f = \left(3 \cdot D_{22} / \zeta' + 12 \cdot D_{66}\right) / L_y^2 \quad \text{when} \quad 1.17 \cdot \zeta' \cdot \sqrt{D_{11} / D_{22}} > 1 \tag{3.38}$$

$$\left(N_{x,cr}\right)_f = \left(\left(7 - 4.12 \cdot \zeta' \cdot \sqrt{D_{11} / D_{22}}\right) \cdot \sqrt{D_{11} \cdot D_{22}} + 12 \cdot D_{66}\right) / L_y^2 \text{ when } 1.17 \cdot \zeta' \cdot \sqrt{D_{11} / D_{22}} < 1 \tag{3.39}$$

Where $\zeta' = D_{22} \cdot L_y / \left(G \cdot J_t\right)$ .

The web buckles first when:

$$\left(N_{x,cr}\right)_f^{SS} \cdot \left(\alpha_{11}\right)_f > \left(N_{x,cr}\right)_w^{SS} \cdot \left(\alpha_{11}\right)_w \tag{3.40}$$

The buckling load is then calculated by expression (3.27).

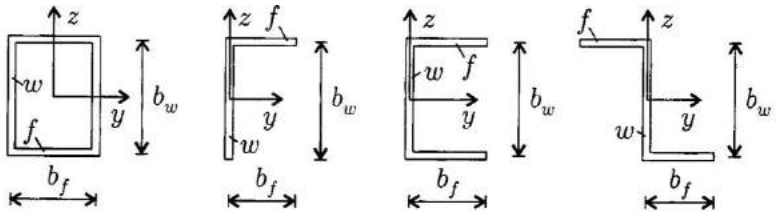


Figure 3.32 Cross-sections of thin-walled members (Kollar 2003, Tarjan et al. 2010)

The buckling loads of the web and flange considered as simply supported (equations. 3.19, 3.20, 3.27, 3.28, 3.34, 3.35) can also be conservatively adopted. This approximation can result in a critical load about 5% to 60% lower (Kollar 2003, Tarjan et al 2010a-b).

Instead of using the previously reported formulations, the critical load can be determined by numerical-analytical procedures, imposing an initial imperfection, i.e. a displacement field proportioned to the first critical mode.

In consideration of the viscoelastic behaviour of the pultruded FRP material, in buckling verifications of members subjected to long-term loading it might be appropriate to adopt reduced values of the elastic constants (see section 3.6.2.2).

## 3.6. **SLS analysis**

In the following the diagrams of the forces and moments in the four frames are reported, for the different serviceability limit state load combinations, and the structural verifications are carried out for some members. In particular, a verification of the stresses and a verification of the maximum deflection are conducted. Only the diagrams in the *x-z* plane are considered. The structural verifications are based on the indications given in (CNR-DT205/2007).

### 3.6.1. **Forces and moments diagrams**

In the following every figure shows the forces and moment diagrams of the structure subjected to the different load combination in x- and y-direction, see Table 3.4. In every scheme the most stressed member is evidenced by a black circle and the related value of the internal action is indicated for the specific frame detailed in Figure 3.1.

### 3.6.1.1. **Axial force**

| | | | |
|---|---|---|---|
| 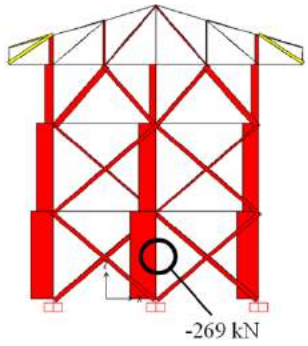 | Frame 1 = -269kN | 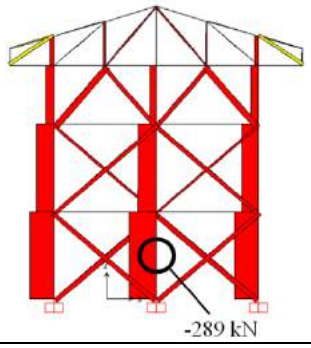 | Frame 1 = -289kN |
| | Frame 2 = -325kN | | Frame 2 = -329kN |
| | Frame 3 = -325kN | | Frame 3 = -321kN |
| | Frame 4 = -269kN | | Frame 4 = -250kN |
| Wind in x-direction | | Wind in y-direction | |

Figure 3.33 Rare load combination, axial force diagrams

| | | | |
|---|---|---|---|
| 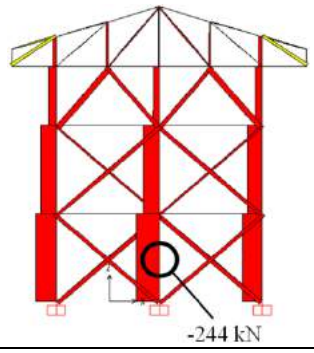 | Frame 1 = -244kN | 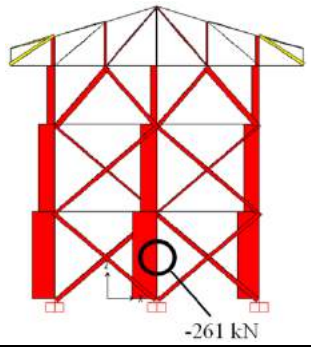 | Frame 1 = -261kN |
| | Frame 2 = -293kN | | Frame 2 = -296kN |
| | Frame 3 = -293kN | | Frame 3 = -290kN |
| | Frame 4 = -244kN | | Frame 4 = -227kN |
| Wind in x-direction | | Wind in y-direction | |

Figure 3.34 Frequent load combination, axial force diagrams

| | | | |
|---|---|---|---|
| 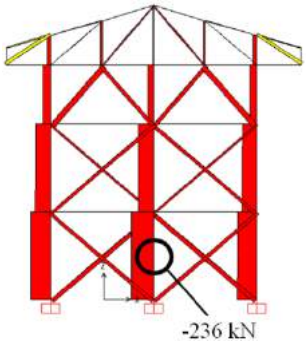 | Frame 1 = -236kN | 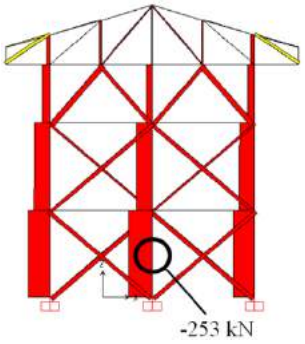 | Frame 1 = -253kN |
| | Frame 2 = -283kN | | Frame 2 = -286kN |
| | Frame 3 = -273kN | | Frame 3 = -279kN |
| | Frame 4 = -236kN | | Frame 4 = -219kN |
| Wind in x-direction | | Wind in y-direction | |

Figure 3.35 Quasi-permanent load combination, axial force diagrams

### 3.6.1.2. **Bending moment**

| | | | |
|---|---|---|---|
| 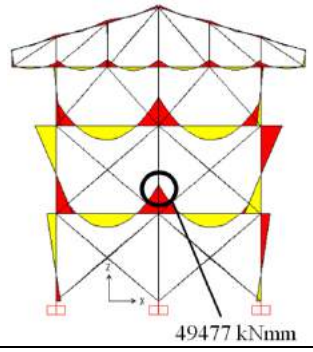 | Frame 1 = 49477kNmm | 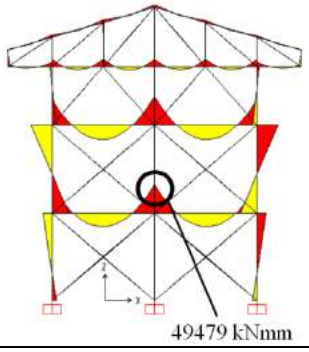 | Frame 1 = 49479kNmm |
| | Frame 2 = 92610kNmm | | Frame 2 = 92611kNmm |
| | Frame 3 = 92611kNmm | | Frame 3 = 92610kNmm |
| | Frame 4 = 49479kNmm | | Frame 4 = 49477kNmm |
| Wind in x-direction | | Wind in y-direction | |

Figure 3.36 Rare load combination, bending moment diagrams

| | | | |
|---|---|---|---|
| 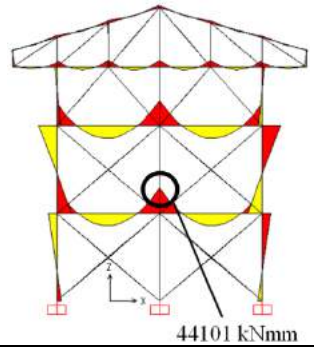 | Frame 1 = 44101kNmm | 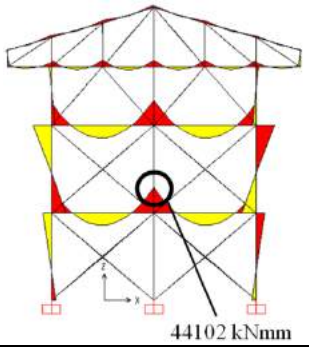 | Frame 1 = 44102kNmm |
| | Frame 2 = 81853kNmm | | Frame 2 = 81853kNmm |
| | Frame 3 = 81853kNmm | | Frame 3 = 81853kNmm |
| | Frame 4 = 44103kNmm | | Frame 4 = 44101kNmm |
| Wind in x-direction | | Wind in y-direction | |

Figure 3.37 Frequent load combination, bending moment diagrams

| | | | |
|---|---|---|---|
| 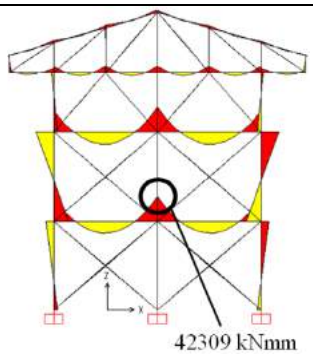 | Frame 1 = 42309kNmm | 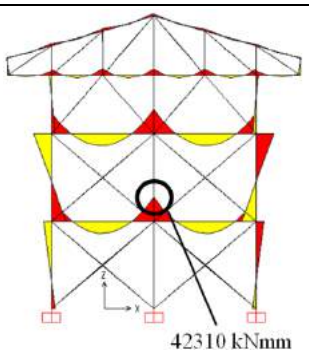 | Frame 1 = 42310kNmm |
| | Frame 2 = 78267kNmm | | Frame 2 = 78267kNmm |
| | Frame 3 = 78267kNmm | | Frame 3 = 78267kNmm |
| | Frame 4 = 42310kNmm | | Frame 4 = 42309kNmm |
| Wind in x-direction | | Wind in y-direction | |

Figure 3.38 Quasi-permanent load combination, bending moment diagrams

### 3.6.1.3. **Shear force**

| | | | |
|---|---|---|---|
| 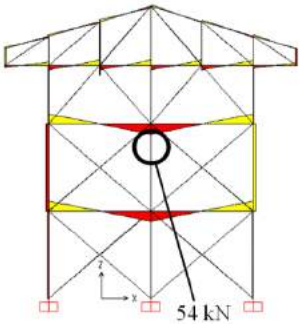 | Frame 1 = 54kN<br>Frame 2 = 103kN<br>Frame 3 = 103kN<br>Frame 4 = 54kN | 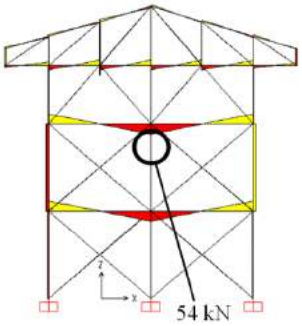 | Frame 1 = 54kN<br>Frame 2 = 103kN<br>Frame 3 = 103kN<br>Frame 4 = 54kN |
| Wind in x-direction | | Wind in y-direction | |

Figure 3.39 Rare load combination, shear force diagrams

| | | | |
|---|---|---|---|
| 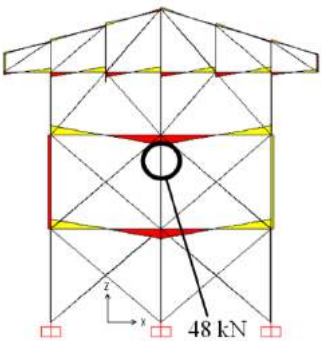 | Frame 1 = 48kN<br>Frame 2 = 91kN<br>Frame 3 = 91kN<br>Frame 4 = 48kN | 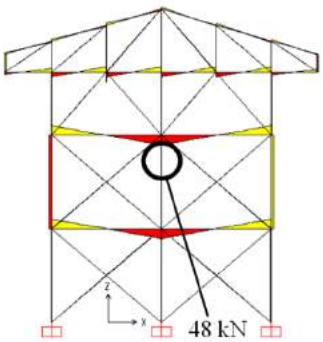 | Frame 1 = 48kN<br>Frame 2 = 91kN<br>Frame 3 = 91kN<br>Frame 4 = 48kN |
| Wind in x-direction | | Wind in y-direction | |

Figure 3.40 Frequent load combination, shear force diagrams

| | | | |
|---|---|---|---|
| 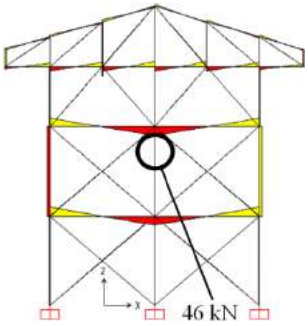 | Frame 1 = 46kN<br>Frame 2 = 87kN<br>Frame 3 = 87kN<br>Frame 4 = 46kN | 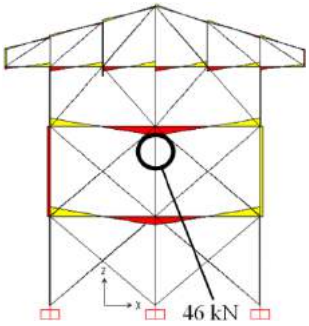 | Frame 1 = 46kN<br>Frame 2 = 87kN<br>Frame 3 = 87kN<br>Frame 4 = 46kN |
| Wind in x-direction | | Wind in y-direction | |

Figure 3.41 Quasi-permanent load combination, shear force diagrams

### 3.6.1.4. **Torsional moment**

| | | | |
|---|---|---|---|
| 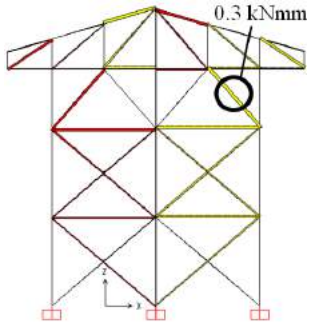 | Frame 1 = 0.3kNmm<br>Frame 2 = 0.01kNmm<br>Frame 3 = 0.02kNmm<br>Frame 4 = 0.3kNmm | 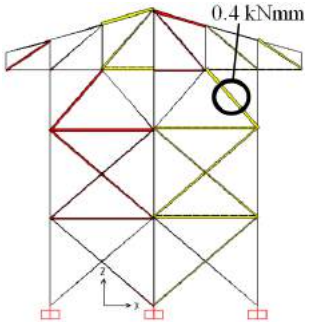 | Frame 1 = 0.4kNmm<br>Frame 2 = 0.03kNmm<br>Frame 3 = 0.005kNmm<br>Frame 4 = 0.3kNmm |
| Wind in x-direction | | Wind in y-direction | |

Figure 3.42 Rare load combination, torsional moment diagrams

| | | | |
|---|---|---|---|
| 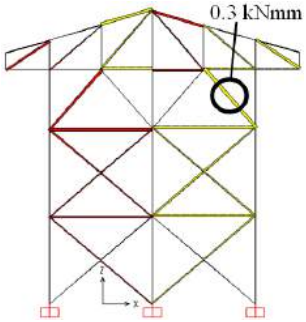 | Frame 1 = 0.3kNmm<br>Frame 2 = 0.02kNmm<br>Frame 3 = 0.02kNmm<br>Frame 4 = 0.3kNmm | 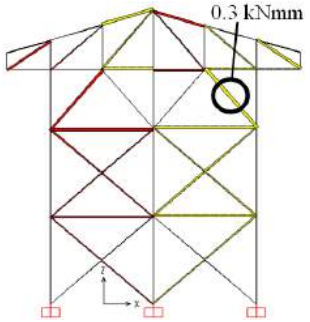 | Frame 1 = 0.3kNmm<br>Frame 2 = 0.03kNmm<br>Frame 3 = 0.009kNmm<br>Frame 4 = 0.3kNmm |
| Wind in x-direction | | Wind in y-direction | |

Figure 3.43 Frequent load combination, torsional moment diagrams

| | | | |
|---|---|---|---|
| 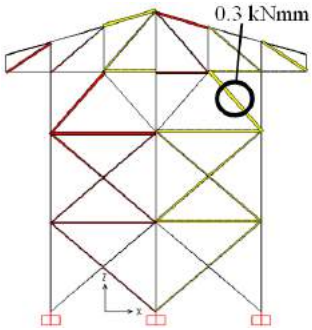 | Frame 1 = 0.3kNmm<br>Frame 2 = 0.02kNmm<br>Frame 3 = 0.02kNmm<br>Frame 4 = 0.3kNmm | 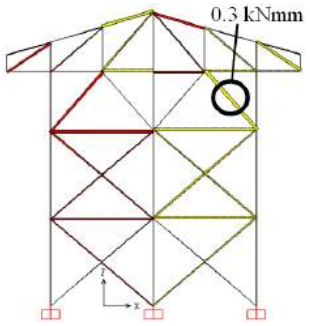 | Frame 1 = 0.3kNmm<br>Frame 2 = 0.03kNmm<br>Frame 3 = 0.01kNmm<br>Frame 4 = 0.4kNmm |
| Wind in x-direction | | Wind in y-direction | |

Figure 3.44 Quasi-permanent load combination, torsional moment diagrams

### 3.6.2. **Verification of elements**

#### 3.6.2.1. **Stresses**

A verification of the compressive stress induced by the axial force and the bending moment is carried out for the column evidenced in Figure 3.45.

| | | | |
|---|---|---|---|
| 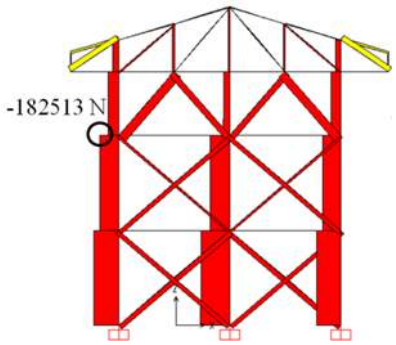 | Frame 3<br>-182,513<br>N | 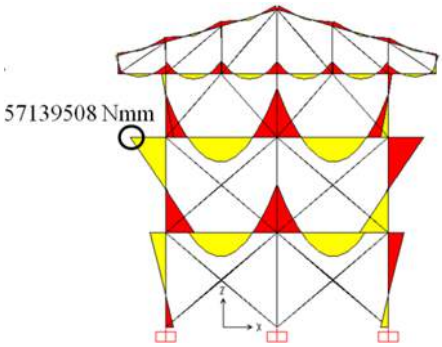 | Frame 3<br>57,139,508<br>Nmm |
| axial force diagram | | bending moment diagram | |
| Wind in x-direction | | | |

Figure 3.45 Quasi-permanent load combination; axial force and bending moment diagrams

It must be verified that the design value of the stress, $f_{Sd}$ , is lower than the limit value, $f_{Rd}$ , defined as follows (CNR-DT205/2007):

$$f_{Rd} = \eta \cdot \frac{f_{Rk}}{\gamma_f} \tag{3.41}$$

where $\eta$ is the conversion factor, $f_{Rk}$ is the characteristic value of the corresponding strength component and $\gamma_f$ is the partial coefficient of the material.

The conversion factor $\eta$ is the product of the environmental factor $\eta_e$ and of the one related to the long-term effects, $\eta_l$.

The mechanical properties of FRP profiles can be degraded in presence of certain environmental conditions: alkaline environment, humidity, extreme temperatures, thermal cycles, ultraviolet radiations. In aggressive environments the value of the environmental factor $\eta_e$ can be assumed equal to 1 if appropriate protective coatings are used. Otherwise the value of $\eta_e$ must be conveniently reduced, also in relation to the design life.

The mechanical properties of FRP profiles can also be degraded due to rheological phenomena (creep, relaxation, fatigue). Values of the conversion factor $\eta_l$ for long-term actions and for cyclic

loading (fatigue) are reported in Table 3.14. In presence of both long-term and cycling loading the overall conversion factor is obtained by the product of the two related conversion factors.

| Type of loading | (SLS) | (ULS) |
|---|---|---|
| Quasi-permanent loading | 0.3 | 1.0 |
| Cyclic loading (fatigue) | 0.5 | 1.0 |

Table 3.14 Values of the conversion factor for long-term effects

The compressive stress induced by the axial force is:

$$f_{Sd,axial} = \frac{N_{Sd}}{A} = \frac{182513}{14100} = 13 \text{ MPa}$$

The compressive stress induced by the bending moment is:

$$f_{Sd,bending} = \frac{M_{Sd}}{W} = \frac{57139508}{1141050} = 50 \text{ MPa}$$

The total compressive stress in the column results:

$$f_{Sd} = f_{Sd,axial} + f_{Sd,bending} = 13 + 50 = 63 \text{ MPa}$$

From equation (3.41) we have:

$$f_{Rd} = (1 \cdot 0.3) \cdot \frac{220}{1} = 66 \text{ MPa}$$

Since $f_{Rd}$ is higher than $f_{Sd}$ the verification is satisfied.

### 3.6.2.2. **Deformations**

For the beam evidenced in Figure 3.46 a verification of the deflection is carried out.

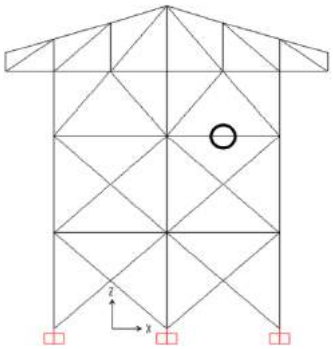

Figure 3.46 The beam for which the deflection analysis is carried out

The deflection of members must be evaluated taking into account the contributions due to flexural and shear deformability.

Deflection limits are reported in Table 3.15. In order to take into account the creep behaviour of the material, the evaluation of the displacements for the quasi-permanent load condition must be conducted adopting reduced values of the elastic constants, with respect to a time equal to the design working life of the structure (CNR-DT205/2007).

Values of the elastic and shear moduli at time *t*, for a load applied at *t*=0, can be computed as:

$$E_L(t) = \frac{E_L}{1+\phi_E(t)} \tag{3.42}$$

$$G_L(t) = \frac{G_L}{1+\phi_G(t)} \tag{3.43}$$

In serviceability limit state, SLS, the action load can be calculated in relationship with the values for the transversal deflection $\eta$ assumed as limitation in design, Tables 3.16 and 3.17.

The values of the creep coefficient for the longitudinal strains, $\phi_E(t)$, and for the shear strains, $\phi_G(t)$, are reported in Table 3.15.

| *t* (time from the application of the load) | $\phi_E(t)$ | $\phi_G(t)$ |
|---|---|---|
| 1 year | 0.26 | 0.57 |
| 5 years | 0.42 | 0.98 |
| 10 years | 0.50 | 1.23 |
| 30 years | 0.60 | 1.76 |
| 50 years | 0.66 | 2.09 |

Table 3.15 Creep coefficient for longitudinal and shear strains (CNR-DT205/2007)

| **Quasi-permanent load combination** | $\delta_{max}$ |
|---|---|
| Floors in presence of plasters, non-flexible partition walls or other brittle finishing materials | *L*/500 |
| Floors without previous limitations | *L*/250 |
| **Rare load combination** | $\delta_{max}$ |
| Footbridges or other structures with an high ratio between accidental and permanent loads | *L*/100 |

Table 3.16 Recommended deflection limits (CNR-DT205/2007)

In Table 3.17 (Clarke 1996) $\eta$ is presented as $\eta_{max}$ and $\eta_1$. $\eta_{max}$ is the maximum deflection while $\eta_1$ is the variation of deflection due to the variable loading increased by time dependent deformations due the permanent load.

| Typical conditions | Limiting values for the vertical deflection | |
|---|---|---|
| | $\eta_{max}$ | $\eta_1$ |
| Walkways for occasional non-public access | Length/150 | Length/175 |
| General non-specific applications | Length/175 | Length/200 |
| General public access flooring | Length/250 | Length/300 |
| Floors and roofs supporting plaster or other brittle finish or non-flexible partitions | Length/250 | Length/350 |
| Floors supporting columns (unless the deflection has been included in the global analysis for the ultimate limit state) | Length/400 | Length/450 |
| Where $\delta_{max}$ can impair the appearance of the structure | Length/250 | - |

Table 3.17 Recommended limiting values for deflection in SLS (Clarke 1996)

In Table 3.18 the formulas for the computation of the maximum deflection $\eta$ of beams taking into account the shear deformability are reported for some common support and loading conditions.

| | | | | | |
|---|---|---|---|---|---|
| **a** | 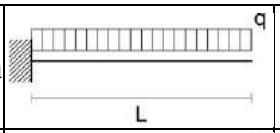 | $\eta_{max} = \frac{q \cdot L^4}{8 \cdot E_L \cdot I} + \frac{q \cdot L^2}{2 \cdot G_L \cdot A_V}$ | **e** | 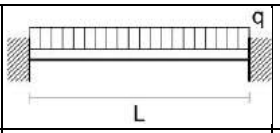 | $\eta_{max} = \frac{q \cdot L^4}{384 \cdot E_L \cdot I} + \frac{q \cdot L^2}{6 \cdot G_L \cdot A_V}$ |
| **b** | 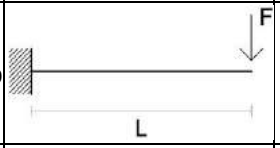 | $\eta_{max} = \frac{F \cdot L^3}{3 \cdot E_L \cdot I} + \frac{F \cdot L}{G_L \cdot A_V}$ | **f** | 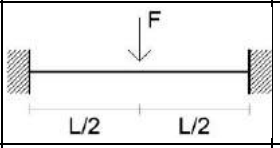 | $\eta_{max} = \frac{F \cdot L^3}{192 \cdot E_L \cdot I} + \frac{F \cdot L}{4 \cdot G_L \cdot A_V}$ |
| **c** | 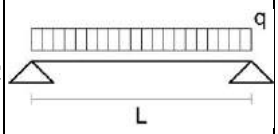 | $\eta_{max} = \frac{5}{384} \cdot \frac{q \cdot L^4}{E_L \cdot I} + \frac{q \cdot L^2}{8 \cdot G_L \cdot A_V}$ | **g** | 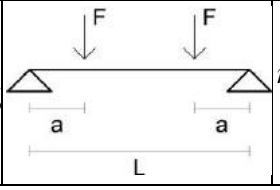 | $\eta_{max} = \frac{F \cdot a}{E_L \cdot I} \cdot \left( \frac{L^2}{8} - \frac{a^2}{6} \right) + \frac{F \cdot a}{G_L \cdot A_V}$ |
| **d** | 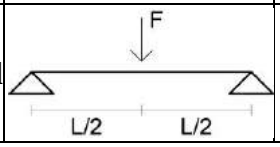 | $\eta_{max} = \frac{F \cdot L^3}{48 \cdot E_L \cdot I} + \frac{F \cdot L}{4 \cdot G_L \cdot A_V}$ | | | |

Table 3.18 Maximum deflection $\eta$ of beams with the shear effects.

The considered beam is subjected to a total distributed load $q$ of 31 N/mm in the quasi-permanent load combination.

Assuming a design working life of 50 years we have, from equations (3.42) and (3.43) and from Table 3.18:

$$E_L(t) = \frac{23000}{1+0.66} = 13855 \text{ MPa}$$

$$G_L(t) = \frac{4500}{1+2.09} = 1456 \text{ MPa}$$

Assuming for the considered beam the static scheme e) of Table 3.18 we have:

$$d_{\max} = \frac{31 \cdot 5400^4}{384 \cdot 13855 \cdot 31400000} + \frac{31 \cdot 5400^2}{6 \cdot 1456 \cdot 4000} = 184 \text{ mm}$$

The computed deflection results significantly larger than the limit of L/250 (22 mm). Adopting, for example, a 500x250x20 mm I-profile the maximum deflection would result 17 mm and the verification would be satisfied.

## 3.7. **Joint's verification**

The verification of the joint represented in Figure 3.47 is carried out in the following. In particular, the verification is carried out for the truss evidenced in the figure, subjected to axial tension. The joint is realized using 14 mm diameter steel bolts that connect the pultruded FRP truss to a laminated FRP plate. The member has a built-up cross-section realized by 2 U 200x60x10 mm. The verification is carried out on base of the indications reported in CNR-DT205/2007.

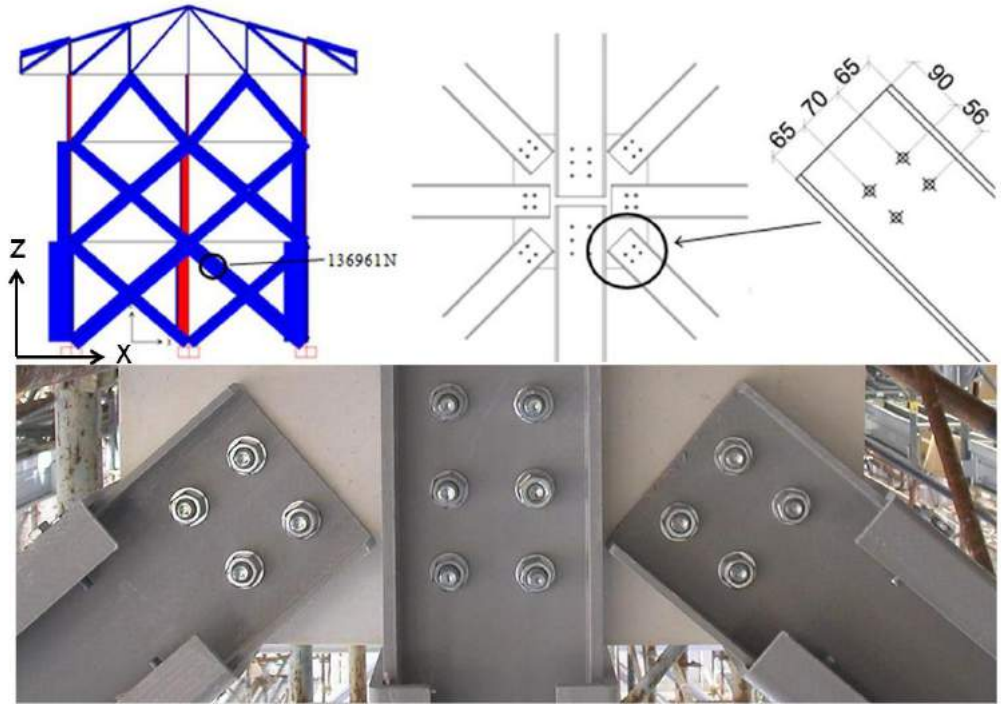


Figure 3.47 Detail of joint (dimensions in millimetres), L'Aquila 2010 (p. 20)

In the case of bolted connections the forces acting on every single bolt can't be evaluated though simple equilibrium criteria, as it is usual in the case of ductile materials.

In general, the bolted connections should meet the following requirements: 1) the barycentric axes of the structural elements should be converge in the same point; 2) with shear action, all bolts must have the same diameter and at least two of them must be arranged in the direction of the load; 3) stiffer washers should be placed under the bolt head and the nut; 4) the bolt torque should be such as to ensure an adequate diffusion of the stresses around the hole; 5) the tightening of the bolts should be take into account the compressive strength of the profile in the direction orthogonal to fibres. The fastening torque must be appropriate to the diameter and class of the bolts; the manufacturers recommend 20-25 Nm.

The geometrical limitations for the bolted connections are summarized in Table 3.19.

| | |
|---|---|
| Bolts diameter | $t_{min} \leq d_b \leq 1.5 \cdot t_{min}$ |
| Holes diameter | $d \leq d_b + 1$ mm |
| Washers diameter | $d_r \geq 2 \cdot d_b$ |
| Distance between holes | $w_x \geq 4 \cdot d_b$; $w_y \geq 4 \cdot d_b$ (Figure 3.48-A) |
| Distance from the end of the plate | $e/d_b \geq 4$; $s/d_b \geq 0.5 \cdot (w_y/d_b)$ (Figure 3.48-A) |

Table 3.19 Geometrical limitations in bolted connections (CNR-DT205/2007)

Where: $d_b$ = diameter of the bolts; $t_{min}$ = thickness of the thinnest joined element; $d$ = diameter of hole; $d_r$ = external diameter; $w_x$ and $w_y$ = distances between the centre of the holes (Figure 3.48-A); $e$ = distance of the bolt from the end of the plate in the direction of the force; $s$ = distance of the bolt from the edge in the direction orthogonal to the force.

In the case in which the resultant of the applied external forces passes through the centroid of the bolting (Figure 3.48-B), it is possible to assign to the bolts forces that are proportional to the coefficients reported in Table 3.20 (CNR-DT205/2007).

| Number of rows | | row 1 | row 2 | row 3 | row 4 |
|---|---|---|---|---|---|
| 1 | FRP/FRP | 120 % | | | |
| | FRP/metal | 120 % | | | |
| 2 | FRP/FRP | 60 % | 60 % | | |
| | FRP/metal | 70 % | 50 % | | |
| 3 | FRP/FRP | 60 % | 25 % | 60 % | |
| | FRP/metal | 60 % | 30 % | 30 % | |
| 4 | FRP/FRP | 40 % | 30 % | 30 % | 40 % |
| | FRP/metal | 50 % | 35 % | 25 % | 15 % |
| > 4 | Not recommended | | | | |

Table 3.20 Shear force distribution coefficients in every bolts row in a bolted connection (CNR-DT205/2007)

### 3.7.1. **Net-tension failure of the plate**

The verification, with respect to normal stresses, of the resisting cross section of the plate weakened due to the presence of the holes results satisfied if the following limitations are respected (CNR-DT205/2007):

- tensile stress parallel to the fibres direction (Figure 3.48-Ca):

$$V_{Sd} \le \frac{1}{\gamma_{Rd}} \cdot f_{Lt,Rd} \cdot (w - n \cdot d) \cdot t \tag{3.44}$$

- tensile stress orthogonal to the fibres direction (Figure 3.48-Cb):

$$V_{Sd} \le \frac{1}{\gamma_{Rd}} \cdot f_{Tt,Rd} \cdot (w - n \cdot d) \cdot t \tag{3.45}$$

where $\gamma_{Rd}$ is the partial coefficient of the model, assumed equal to 1.11 for cross-sections with holes, $V_{Sd}$ is the force transmitted from the bolts to the plate, $f_{Lt,Rd}$ and $f_{Tt,Rd}$ are, respectively, the design value of the tensile strength of the material in the direction parallel to fibres and in the direction orthogonal to the fibres, $t$ is the thickness of the element and $n$ is the number of holes.

For the case in exam, since we have two bolt rows, the shear force in every row results, from Table 3.20, $V_{Sd} = 136961 \cdot 0.6 = 82177$ N

From equation (3.44) we obtain:

$$\frac{1}{1.11} \cdot 268 \cdot (200 - 2 \cdot 14) \cdot 20 = 830559 \text{ N} > 82177 \text{ N}$$

so the verification is satisfied.

### 3.7.2. **Shear-out failure of the plate**

The verification with respect to the shear-out failure mode (Figure 3.48-D) results satisfied if the following limitation is respected (CNR-DT205/2007):

$$V_{Sd} \le f_{V,Rd} \cdot (2 \cdot e - d) \cdot t \tag{3.46}$$

where $f_{V,Rd}$ is the design value of the shear strength of the FRP element.

For the case in exam we have, from equation (3.46):

$27 \cdot (2 \cdot 90 - 14) \cdot 20 =$ 89640 N > 82177 N

so the verification is satisfied.

### 3.7.3. **Bearing failure of the plate**

In the verification with respect to the bearing failure of the plate, the mean value of the pressure exerted by the bolt shank on the walls of the hole must satisfy the following limitations (CNR-DT205/2007):

- stress parallel to the fibres direction (Figure 3.48-Ea):

$$V_{Sd} \le f_{Lr,Rd} \cdot d_b \cdot t \tag{3.47}$$

- stress orthogonal to the fibres direction (Figure 3.48-Eb):

$$V_{Sd} \le f_{Tr,Rd} \cdot d_b \cdot t \tag{3.48}$$

where $f_{Lr,Rd}$ and $f_{Tr,Rd}$ are, respectively, the design value of the bearing strength of the material in the directions parallel and orthogonal to the fibres.

For the case in exam we have, from equation (3.47):

$147 \cdot (14 \cdot 2) \cdot 20 =$ 82320 N > 82177 N

so the verification is satisfied.

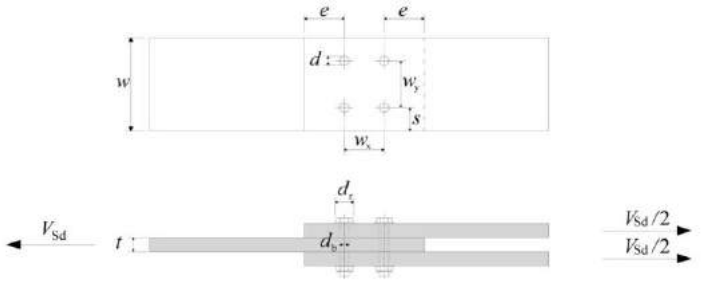


(A) Bolted connection *(CNR-DT205/2007)*

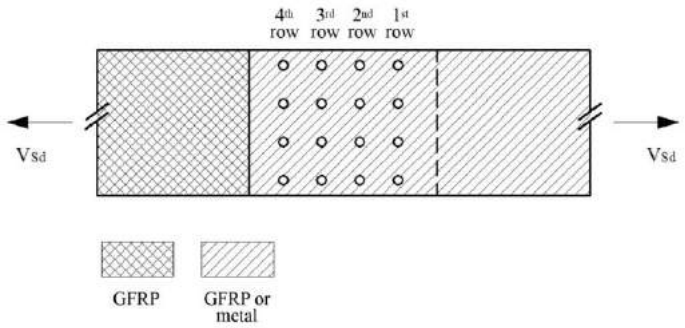


(B) Arrangement of the bolts rows in a bolted connection between two FRP plates or between a FRP plate and a metal one. The resultant of the external forces passes through the centroid of the bolting (CNR-DT205/2007)

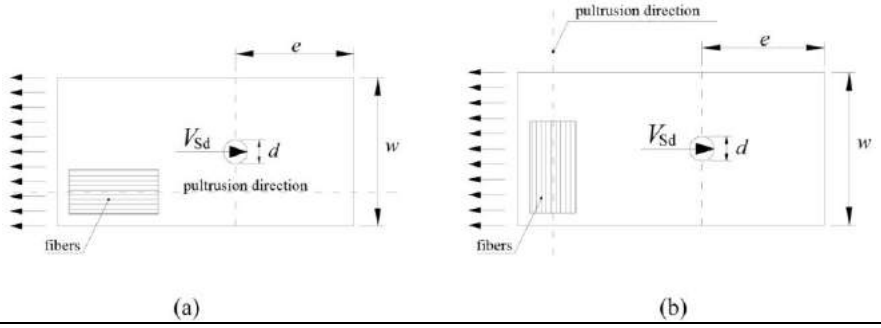


(C) Net-tension failure mode (CNR-DT205/2007)

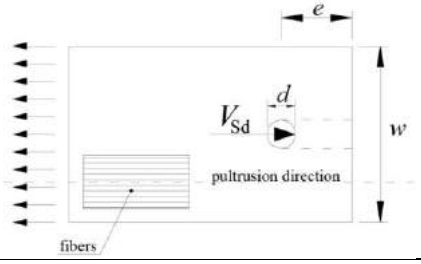


(D) Shear-out failure mode (CNR-DT205/2007)

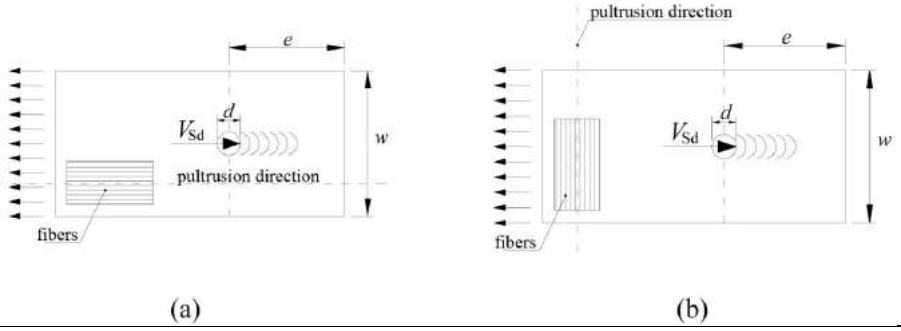


(E)_Bearing failure mode (CNR-DT205/2007)

Figure 3.48 Verification of the joints; schemes reported in CNR-DT205/2007

Figure 3.49

### 3.7.4. **Shear failure of the steel bolt**

The verification with respect to the shear failure of the steel bolt results satisfied if the following limitation is respected (CNR-DT205/2007):

$$V_{Sd} \leq f_{Vb,Rd} \cdot A_b \tag{3.49}$$

where $f_{Vb,Rd}$ represents the design value of the shear strength of the bolt, as defined in current standards, and $A_b$ is the resistance area of the cross-section of the bolt.

For the case in exam we have:

$$f_{Vb,Rd} = \frac{0.6 \cdot f_{ub}}{\gamma_{M2}} = \frac{0.6 \cdot 800}{1.25} = 384 \text{ MPa}$$

In previous equation $f_{ub}$ is the tensile strength of the bolt and $\gamma_{M2}$ is the partial safety factor.

Since the shear force acting on every bolt is $V_{Sd} = 82177/2 =$ 41089 N, we have, from equation (3.49):

$384 \cdot 115 =$ 44160 N > 41089 N

so the verification is satisfied.

## 3.8. **References**

Ascione, L., Giordano, A. and Spadea, S., Lateral buckling of pultruded FRP beams, Composites Part B: Engineering, 42 4, 2011, 819-824.

Ascione, L., Berardi, V.P., Giordano, A. and Spadea, S., Buckling failure modes of FRP thin-walled beams, Composites Pt B: Engineering, 47, 2013, 357-364. DOI: 10.1016/j.compositesb.2012.11.006

Ascione, L. Berardi, V.P., Giordano, A. and Spadea, S., Local buckling behavior of FRP thin-walled beams: A mechanical model, Composite Structures, 98, 2013, 111–120.

Ascione, L., Berardi, V.P. and Spadea, S., Macro-scale analysis of local and global buckling behavior of T and C composite sections, Mechanics Research Communications (Special Issue), 58, 2014, 105-111. http://www.sciencedirect.com/science/article/pii/S0093641313001614

Ascione, L., Berardi, V.P., Giordano, A. and Spadea, S., Pre-buckling imperfection sensitivity of pultruded FRP profiles, Composites Part B – Engineering, 72, 2015, 206-212.

Bank LC. Composites for construction-structural design with FRP materials, John Wiley & Sons, NJ, 2006.

Bartbero, E.J., De Vivo, L., Beam-Column Design Equation for Wide-Flange Pultruded Structural Shapes, Journal of Composite for Construction, Vol. 3, n. 4 (1999), pp. 185-191.

Boscato, G., and Russo, S. Dissipative capacity on FRP spatial pultruded structure, Composite Structures, 2014; Volume 113(7), p.339–353.

Chopra AK. Dynamics of structures, 3rd Ed., Pearson Prentice Hall, 2007.

Clarke JL. (Ed.). EUROCOMP design code and handbook: Structural design of polymer composites, E & FN Spon, London, 1996.

CNR-DT205/2007 Guide for the design and constructions of structures made of FRP pultruded elements, National Research Council of Italy, Advisory Board on Techincal Recommendations. http://www.cnr.it/sitocnr/IlCNR/Attivita/NormazioneeCertificazione/DT205_2007.html.

Creative pultrusions design guide,' Creative Pultrusions, Inc., Alum Bank, Pa, 1988.

Engesser, F. (1889). "Ueber die Knickfestigkeit gerader Stabe", Zeitschrift für Architekter und Ingenieurwsen, 35(4), 455-462 (in German).

Eurocode 1: Basis of structural design. EN 1990:2002 (E)

Eurocode 3: Design of steel structures - Part 1-1: General rules. ENV 1993-1-1: 1992. Incorporating Corrigenda February 2006 and March 2009.

Eurocode 8 Design of structures for earthquake resistance. Part 1: General rules, seismic actions and rules for buildings. EN1998-1:2004 (E),: Formal Vote Version (Stage 49), 2004.

Feroldi, F. and Russo, S. (2016). Structural Behavior of All-FRP Beam-Column Plate-Bolted Joints. J. Compos. Constr. ,10.1061/(ASCE)CC.1943-5614.0000667, 04016004.

Girão Coelho, A.M. and Mottram, J.T., 'A review of the behaviour and analysis of mechanically fastened joints in pultruded fibre reinforced polymers,' Materials & Design, 74, (2015), 86-107. ISSN: 0261-3069

Girão Coelho, A.M., Mottram J.T. and Harries, K.A., Bolted connections of pultruded GFRP: Implications of geometric characteristics on net section failure, Composite Structures, 131, (2015), 878-884. http://dx.doi.org/10.1016/j.compstruct.2015.06.048

Mottram, J.T., Lateral-torsional buckling of thin-walled composite I-beams by the finite difference method, Composites Engrg., 2 2, 1992, 91-104.

Mottram, J.T., Lutz, C., and Dunscombe, G.C., Aspects on the behaviour of bolted joints for pultruded fibre reinforced polymer profiles, International Conference on Advanced Polymer Composites for Structural Applications in Construction (ACIC04), Woodhead Publishing, Cambridge, 348-391.

NTC08. Norme Tecniche per le Costruzioni (last update of the Italian Building Code), Decree of the Ministry of Infrastructures of 14th January 2008. (in Italian).

Pecce, M. and Cosenza, E., Local buckling curves for the design of FRP profiles, Thin-Walled Structures, 37 3, 2000, 207-222.

Pecce, M. and Cosenza, E., FRP structural profiles and shapes, in Wiley. Encyclopedia of Composites, 2012 - Wiley Online Library.

Poursha M, Khoshnoudiana F, Moghadam A.S. A consecutive modal pushover procedure for estimating the seismic demands of tall buildings. Engineering Structures 31 (2009) 591_599.

Poursha M, Khoshnoudiana F, Moghadam A.S. A consecutive modal pushover procedure for nonlinear static analysis of one-way unsymmetric-plan tall building structures. Engineering Structures 33 (2011) 2417–2434.

Priestley M.J.N., Calvi, M.C., and Kowalsky, M.J. (2007) Displacement-Based Seismic Design of Structures IUSS Press, Pavia, 670 pp.

Russo, S., Experimental and finite element analysis of a very large pultruded FRP structure subjected to free vibration, Compos. Struct., 2012; 94(3): 1097–1105.

SAP2000 Advanced v. 10.1.2. Structural Analysis Program, Computers and Structures, Inc., 1995 University Ave, Berkeley, CA.

Kollar L.P., Local Buckling of Fiber Reinforced Plastic Composite Structural Members with Open and Closed Cross Section. Journal of Structural Engineering, ASCE, 2003. 129: 1503-1513.

Tarjan, G., Sapkas, A. and Kollar, L.P. Local Web Buckling of Composite (FRP) Beams. Journal of Reinforced Plastics and Composites, Vol. 29, No. 10/ 2010.

Tarjan, G., Sapkas, A. and Kollar, L.P. Stability Analysis of Long Composite Plates with Restrained Edges Subjected to Shear and Linearly Varying Loads, J. of Reinf. Plastics and Comp., Vol. 29, No. 9/ 2010.

Turvey GJ, Cooper C. Review of tests on bolted joints between pultruded GRP profiles. Proceedings of the Institution of Civil Engineers Structures & Buildings 157, June 2004 Issue SB3. p. 211–233.

## 4. FINAL EVALUATION FOR DESIGN OF FRP STRUCTURES IN SEISMIC ZONE

Overview

The absence of specific calculation codes for the seismic design of FRP structures implies that the most restrictive parameters must be taken. The behaviour factor $q$ is calibrated with the real material characteristics and structural types (therefore with $q$ = 1 and damping coefficient $\zeta$=5%, as suggested by Eurocode 8 (2004) and NTC08 (2008)); this leads to a conservative calculation approach.

The low density of the FRP material (1700-1900 kg/m³) is a fundamental point in seismic design, since it brings a spontaneous reduction of the seismic actions and a limited participating mass and acceleration.

This feature must be opportunely managed in the design phase by adopting appropriate boundary conditions at the base and/or stabilizing loads at different heights, to withstand the horizontal displacements.

On the basis of some researches (Boscato and Russo 2014) the low frequencies of the vibration modes and the limited dissipation capacity of FRP structures ($1.5<\zeta<2$) must be accounted for, with reference to the seismic characteristics of the soil.

The increment of flexural deformability with the height of FRP structures tends to increase the period of vibration $T_{0.}$

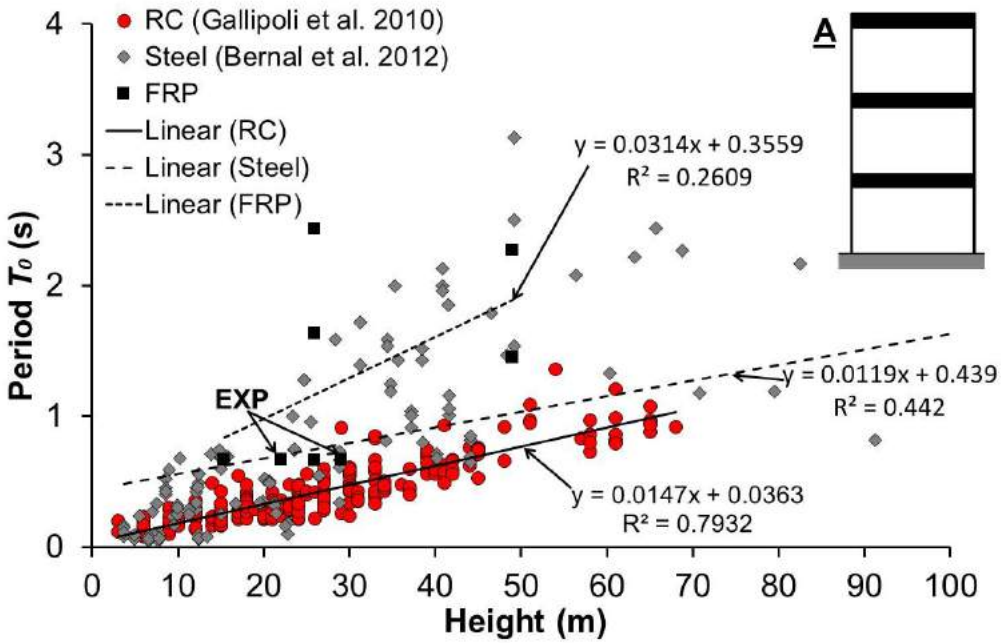


Figure 4.1. Fundamental period of RC, Steel and FRP structures (detail A)

The fundamental periods $T_0$ (Sheet 3) of different FRP structures have been compared with traditional materials, such as RC (Reinforced Concrete) and Steel, in Figure 4.1.

As regards the FRP structures two $T_0$-height relationships are experimental values (labeled EXP), while the others have been calculated by numerical model. The best linear relation concerns the RC structures having the $R^2$ (coefficient of determination) value closest to 1, while for FRP and steel the $R^2$ value is less than 0.5 highlighting the scattering of results due to the high variability of the mechanical-physical-geometrical characteristics. The linear regressions of FRP and steel structures show the tendency to high period of vibration due to the greater deformability of these structures with respect to RC buildings.

When an earthquake's PGA (Peek Ground Acceleration) happens along a period shorter than 0.5 s, FRP structures - that are characterized by a long vibration period - keep on moving in free vibrations that slowly damp and avoid resonance between the time-delayed response of the structure and the fast one of stiff types of soil (i.e. A and B types).

Since that the high deformability could be faced with an over dimensioning of the FRP elements and so over passing the above prudential approach a detailed preliminarily Design by Testing phase is judged necessary, to assess the parameters and coefficients that identify the dynamic structural response of FRP structures.

The results of the first study conducted on the damping value of the mono-dimensional elements (Boscato 2011, Boscato and Russo 2009) and of the FRP structures (Boscato and Russo 2014) are particularly interesting when compared with the values recorded in the following table defined by Chopra (1995) and Newmark and Hall (1982) which refers to traditional materials, Tables 4.1 and 4.2.

| *Structure typologies and boundary conditions* | *ζ* |
|---|---|
| *Structures with elements below of 50% than elastic limit* | |
| *RC Structures with first cracks*<br>*RC Prestressed Structures*<br>*Welded steel structures* | *2-3%* |
| *RC Structures cracked* | *3-5%* |
| *Bolted or nailed steel structures*<br>*Bolted or nailed wood structures* | *5-7%* |
| *Structures with elements near to elastic limit* | |
| *RC Prestressed Structures without pretension loss*<br>*Welded steel strutures* | *5-7%* |
| *RC Prestressed Structures*<br>*RC Structures* | *7-10%* |
| *Bolted or nailed steel structures*<br>*Bolted wood structures* | *10-15%* |
| *Nailed wood structures* | *15-20%* |
| *Masonry structures* | |
| *Normal masonry structures* | *3%* |
| *Reinforced masonry structures* | *7%* |

Table 4.1. Damping coefficients ζ; Chopra (1995) and Newmark and Hall (1982)

| *Structure typologies and boundary conditions* | *ζ* |
|---|---|
| *Members* | |
| *Columns with fixed boundary conditions* | *2.5%* |
| *Beams with supported boundary conditions* | *2.5-3.5%* |
| *Structures* | |
| *Structures with bolted beam-column connections* | *1.3%* |

Table 4.2. Damping coefficients ζ for pultruded FRP elements and structures

Nevertheless, in the design phase, the structure's maximum displacements must be evaluated with reference to the design earthquake and thus to the soil characteristics. For such highly deformable structures, the absolute displacement of the whole mass is null under the inertial force, while the relative displacement referred to the soil is maximum and opposite.

General recommendations

This document contains general rules for earthquake-resistant design of FRP buildings and should be used in conjunction with CNR-DT205/2007, CEN TC250 WG4L and Sections 2 to 4 of EN 1998-1 and, finally, Chapter 7 of NTC08.

For the performance requirements and compliance criteria of structures, Section 2 of EN 1998-1 and NTC08 should be applied.

For the ground conditions and seismic action, Section 3 of EN 1998-1 and Chapter 3.2 of NTC08 must be applied.

For the general rules of design of structures, Section 4 of EN 1998-1 and Chapter 7 of NTC08 should be taken into account.

Design concepts

Earthquake resistant pultruded FRP structures should be designed in accordance with one of the following design concepts (Table 4.3):

a) Low-dissipative structural behaviour for conservative approach

b) Dissipative structural behaviour

| Design concept | Structural Ductility Class |
|---|---|
| a) Low dissipative structural behaviour | DCL (Low) |
| b) Dissipative structural behaviour | DCM (Medium) |
| | DCH (High) |

Table 4.3. Structural ductility classes (EC8, EN 1998-1:2004)

In design concept a) the action effects may be calculated on the basis of an elastic global analysis without taking into account the dissipative behaviour of pultruded FRP structure offered by bolted joints. In the case of irregularity in elevation the behaviour factor *q* should be corrected as indicated in §2.2.5.3 but it needs to be taken smaller than minimum value. The resistance of the members and of the connections should be assessed in accordance with CNR-DT205/2007 and NTC08. The capability of parts of the structure to resist earthquake actions out of their elastic range is taken into account. A structure belonging to a given ductility class should meet specific requirements in one or more of the following two aspects: structural type and rotational capacity of connections.

In design concept b) the capability of parts of the structure to resist and dissipate the earthquake actions through the strength hierarchy criteria is taken into account. Structures designed in accordance with design concept b) should belong to structural ductility classes DCM or DCH. These classes correspond to increased ability of the structure to dissipate energy through mechanisms that involve the global structure. Depending on the ductility class, specific requirements in one or more of the following aspects should be met: global geometry, strength hierarchy criteria and rotational capacity of joints and connections.

Structural types

All-FRP buildings should be assigned to one of the structural types outlined in EN 1998-1, Section 6.3 according to the behaviour of their primary resisting structure under seismic actions:

a) Moment resisting frame (see EN 1998-1, Section 6.3);

b) Frames with concentric bracings (see EN 1998-1, Section 6.3);

d) Moment resisting frames combined with concentric bracings (see EN 1998-1, Section 6.3);

e) Structures with stiff cores or walls (see EN 1998-1, Section 6.3).

Behaviour factor

For regular pultruded FRP structures the behaviour factor *q* is listed in Table 4.4.

| **Structural Ductility Class** | **Behaviour factor *q*** |
|---|---|
| DCL (Low) | 1 |
| DCM (Medium) | 1-1.5 |
| DCH (High) | >1.5 |

Table 4.4. Behaviour factors

For non-regular structures in elevation (see EN 1998-1, Section 4.2.3.3) the *q*-values listed in Table 5.2 should be reduced by 20%, but don't need to be taken lower than $q$=1.

For structures having different and independent properties in the two horizontal directions, the *q* factors to be used for the calculation of the seismic action effects in each main direction should correspond to the properties of the structural system in the analyzed direction and then can be different.

A conservative design approach is adopted in the manual with the consequence upon the choice of the force reduction factor and of the damping coefficients required to define the response spectra.

Advices and precautions

In absence of ductile behaviour for brittle failure of pultruded FRP material, the ratio between the residual strength after degradation and the initial one should be taken into account. The global dissipative response of aforementioned design concept b is assumed to be due to the progressive response of different parts involved by consecutive failure mechanisms through the strength hierarchy criteria. Moment resisting frames combined with concentric bracings are recommended in FRP structures to withstand horizontal actions. Dissipative zones should be located in joints and connections, whereas the pultruded FRP members themselves should be regarded as behaving elastically. The damage propagation in FRP pultruded bolted joints could be taken into account through a design by testing at the preliminary phase.

With soil classes of low stiffness (C, D or E classes, see Eurocode 8 and NTC08), the constant acceleration branch of the spectrum (from $T_b$ to $T_c$) - and thus also the soil's fundamental period of resonance - increases. Taking into account the high vibration periods of FRP structures (about >0.65 s), the design in presence of soils with a large frequency band of the acceleration plateau must address the increase in eigenfrequencies (with a stiffness increase by inserting bracings) or the increase in participating mass to avoid resonance in the soil-to-structure interaction.

The seismic design must account above all for second order phenomena that regard particularly FRP members. Besides, dynamic actions induce member stress inversion that must be carefully evaluated with reference to the high deformability of the material and to the higher vulnerability (weakness) of FRP profiles in compression than in tension.

Even if not yet defined from clear rules and recommendations, the high deformability of FRP structures suggests to limit the framed building to 2-3 floors with an interstory height of circa 3meters; this is due in order to exalt a conservative approach while waiting for more studies especially on full size FRP structures.

The results of the verifications put in evidence some of the critical aspects of the structural behaviour of pultruded FRP profiles. In particular, deformation and buckling limit states, rather than material strength limits, frequently govern the design of FRP structural shapes because of their low moduli and anisotropic behaviour. Moreover, the high shear deformability of the pultruded material can also have a significant influence on the buckling behaviour. In fact, for the examined case, the compression buckling check didn't result satisfied, as well as the deflection check at the serviceability limit state. Another critical aspect can regard the verification of the shear stress. In fact, the shear response of pultruded FRP profiles is governed by the resin's characteristics, resulting in relatively low shear strength of the composite material. On the contrary, the material performance in the longitudinal direction mostly depends on the fibre's characteristics, thus showing very high values of the compressive and, especially, tensile strength.

Design strategies for enhanced seismic performance

For design purposes in order to achieve a dissipative response the following basic conditions must be satisfied:

- base column connections, beam-to-column joints and bracing details must be designed in order to sustain the anticipated cyclic deformation demand, without strength degradation or local failure, so that the lateral strength and dissipative capacity is maintained during the seismic action;

- a specific over-strength of structural elements and strength hierarchy must be taken into account in order to preserve the structural integrity under seismic action;

- only the concentrically braced configuration assures a better dynamic response of the frame. The moment resisting frame must be solved with an over-strength design of structural elements and joints. The combination of aforementioned configurations - moment resisting frame and concentric bracings - guarantees a better seismic behavior both in term of resistance and dissipative capacity through the interactive response;

- failure mechanisms triggered by local buckling and net section fracture preclude the global ductile behavior. Mitigation of all potentially undesirable failure modes through appropriate detailing is required to achieve good seismic performance;

- with regard to the FRP structure, characterized by elastic-brittle material, it is important to design the collapse mechanism at the desired locations prior to the occurrence of other failure modes;

- the global second order effects (P-Δ) must be taken into account in the design phase to avoid the amplification of drift. Considering the low self-weight these structures must possess sufficient lateral stiffness and strength to control the deformation demand from earthquake;

- phases of progressive damage under repeated loading can be taken into account in design stage to provide a global ductile response;

- several structural configurations can be adopted to reduce the seismic loads: moment resisting frame MRF with dissipative point in beam-to-column joint, combination with shear walls, concentrically braced frames CBF, buckling-restrained frames, eccentrically braced frames;

- frames with concentric V-bracings should be avoided. This configuration makes the beams work in shear, then in the weakest direction.

## 4.1. **References**

Bernal D, Kojidi SM, Kwan K, Döhler M, 2010. Damping identification in buildings from earthquake records. SMIP12 SEMINAR PROCEEDINGS.

G. Boscato, S. Russo (2009). Free Vibrations of Pultruded FRP Elements: Mechanical Characterization, Analysis, and Applications. ASCE Journal of Composite for Construction, 13 (6), pp. 565-574.

Boscato G. (2011). Dynamic behaviour of GFRP pultruded elements. Published by University of Nova Gorica Press, P.O. Box 301, Vipavska 13, SI-5001 Nova Gorica, Slovenia. ISBN 978-961-3611-68-7.

Boscato, G., and Russo, S. Dissipative capacity on FRP spatial pultruded structure, Composite Structures, 2014; Volume 113(7), p.339–353.

CEN TC250 WG4L, Ascione, J-F. Caron, P. Godonou, K. van IJselmuijden, J. Knippers, T. Mottram, M. Oppe, M. Gantriis Sorensen, J. Taby, L. Tromp. Editors: L.Ascione, E. Gutierrez, S. Dimova, A. Pinto, S. Denton. 'Prospect for New Guidance in the Design of FRP,' Support to the implementation and further development of the Eurocodes, JRC Science and Policy Report JRC99714, EUR 27666 EN, European Union, Luxembourg, (2016), p 171. ISBN 978-92-79-54225-1 doi:10.2788/22306

Chopra AK. Dynamics of structures, 3rd Ed., Pearson Prentice Hall, 2007.

CNR-DT205/2007 Guide for the design and constructions of structures made of FRP pultruded elements, National Research Council of Italy, Advisory Board on Techincal Recommendations. http://www.cnr.it/sitocnr/IlCNR/Attivita/NormazioneeCertificazione/DT205_2007.html.

Eurocode 8 Design of structures for earthquake resistance. Part 1: General rules, seismic actions and rules for buildings. EN1998-1:2004 (E),: Formal Vote Version (Stage 49), 2004.

Gallipoli M.R., Mucciarelli M., Šket-Motnikar B., Zupančić P., Gosar A., Prevolnik S., Herak M., Stipčević J., Herak D., Milutinović Z., Olumćeva T., (2012). Empirical estimates of dynamic parameters on a large set of European buildings, Bulletin of Earthquake Engineering, 8, pages: 593 – 607.

Newmark, N.M., Hall, W.J., Earthquake spectra and design, Earthquake Engineering Research Institute, Berkeley, California, 1982.

NTC08. Norme Tecniche per le Costruzioni (last update of the Italian Building Code), Decree of the Ministry of Infrastructures of 14th January 2008. (in Italian).

## 4.2. **Symbols**

$Station$ = output station

$COMB$ = load combination

$N_{Sd}$ = design value of the acting normal force

$V_{2,Sd}$ = design value of the acting shear force in direction 2

$V_{3,Sd}$ = design value of the acting shear force in direction 3

$T_{Sd}$ = design value of the acting torsional moment

$M_{2,Sd}$ = design value of the acting bending moment around axis 2

$M_{3,Sd}$ = design value of the acting bending moment around axis 3

Shape = cross-section shape

$t_3$ = height of the cross-section

$t_2$ = width of the cross-section

$t_f$ = thickness of the flange

$t_w$ = thickness of the web

$A$ = area of the cross-section

$I_t$ = torsional constant

$I_{33}$ = moment of inertia with respect to axis 3

$I_{22}$ = moment of inertia with respect to axis 2

$A_{S2}$ = shear area in direction 2

$A_{S3}$ = shear area in direction 3

$W_{33}$ = section modulus with respect to axis 3

$W_{22}$ = section modulus with respect to axis 2

$E_1$ = longitudinal elastic modulus in direction 1

$E_2$ = transverse elastic modulus in direction 2

$E_3$ = transverse elastic modulus in direction 3

$G_{12}$ = shear modulus in direction 1-2

$G_{13}$ = shear modulus in direction 1-3

$G_{23}$ = shear modulus in direction 2-3

$\nu_{12}$ = Poisson ratio in direction 1-2

$\nu_{13}$ = Poisson ratio in direction 1-3

$\nu_{23}$ = Poisson ratio in direction 2-3

$\eta_e$ = environmental factor (default = 1)

$\eta_{l,ULS}$ = factor related to the long-term effects for ultimate limit states (default = 1) (see Table 5.1)

$\eta_{l,SLS}$ = factor related to the long-term effects for serviceability limit states (default = 0.3) Table 5.1)

| **Type of loading** | $\eta_{l,SLS}$ | $\eta_{l,ULS}$ |
|---|---|---|
| Quasi-permanent loading | 0.3 | 1.0 |
| Cyclic loading (fatigue) | 0.5 | 1.0 |

Table 5.1 Values of the conversion factor for long-term effects

$\gamma_{f1,ULS}$ = partial coefficient of the material related to the uncertainty level in the determination of the material properties for ultimate limit states (default = 1.15) (see Table 5.2)

$\gamma_{f1,SLS}$ = partial coefficient of the material related to the uncertainty level in the determination of the material properties for serviceability limit states (default = 1) (see Table 5.2)

$\gamma_{f2,ULS}$ = partial coefficient of the material related to the brittle behavior for ultimate limit states (default = 1.3) (see Table 5.2)

$\gamma_{f2,SLS}$ = partial coefficient of the material related to the brittle behavior for serviceability limit states (default = 1) (see Table 5.2)

| **Value of the coefficient of variation for the material properties $V_x$** | $\gamma_{f1,ULS}$ | $\gamma_{f1,SLS}$ | $\gamma_{f2,ULS}$ | $\gamma_{f2,SLS}$ |
|---|---|---|---|---|
| $V_x \leq 0.10$ | 1.10 | 1.0 | 1.3 | 1.0 |
| $0.10 < V_x \leq 0.20$ | 1.15 | 1.0 | 1.3 | 1.0 |

Table 5.2 Values of the partial coefficient of the material

$\gamma_{Rd}$ = partial coefficient that takes into account the uncertainties related to the mechanical model (default = 1.11)

*t* = target time for long-term deformations verifications (default = 0) (see Table 5.3)

| **Structural type** | *t* (years) |
|---|---|
| Temporary structures | 10 |
| Ordinary structures | 50 |

Table 5.3 Target time for deformation verifications of different structural types

$f_{t,k}$ = characteristic value of the longitudinal tensile strength of the material (default = 250)

$f_{c,k}$ = characteristic value of the longitudinal compressive strength of the material (default = 250)

$f_{V,k}$ = characteristic value of the shear strength of the material (default = 35)

$E_{Lc}$ = longitudinal elastic modulus in compression (default = $E_1$)

$E_{Tc}$ = transversal elastic modulus in compression (default = $E_2$)

$c$ = coefficient used for the stability verifications of double-T profiles (default = 0.65)

$E_{eff}$ = effective longitudinal elastic modulus (default = $E_1$)

$G_{eff}$ = effective shear modulus (default = $G_{12}$)

$n$ = number of holes (default = 0)

$d$ = diameter of holes (default = 0)

$t$ = thickness of the profile (default = 0)

$K_c$ = multiplicative coefficient of the length of the member, for stability verifications in compression (default = 1) (see Table 5.4)

| **1st extremity support condition** | **2nd extremity support condition** | $K_c$ |
|---|---|---|
| Fixed | Free | 2 |
| Hinged | Hinged | 1 |
| Fixed | Hinged | 0.8 |
| Fixed | Fixed | 0.7 |

Table 5.4 Values of coefficient $K_c$ for single structural members. For members of a frame the value of $K_c$ should be evaluated as indicated in Eurocode 3

$z_q$ = coordinate of the point of application of the load with respect to the center of gravity of the cross-section (default = $t_3/2$)

$K_f$ = multiplicative coefficient of the length of the member, for stability verifications in flexure (unbraced length of the member = $K_f \cdot L$) (default = 1)

$C_1$ = coefficient used for the flexural stability verifications of double-T profiles (default = 1.13)

$C_2$ = coefficient used for the flexural stability verifications of double-T profiles (default = 0.45)

$C_3$ = coefficient used for the flexural stability verifications of double-T profiles (default = 1)

$k_{f2}$ = coefficient used for the flexural stability verifications of box and pipe profiles (default = 1)

Static scheme = static scheme for the computation of the deflection (default = c)

$F$ = value of the applied force for the computation of the deflection (default = 0)

$q$ = value of the applied distributed load for the computation of the deflection (default = 0)

$a$ = distance between the points of application of the load and the extremities of the beam, for the computation of the deflection (default = 0)

$\eta_{ULS}$ = conversion factor for ultimate limit states

$\eta_{SLS}$ = conversion factor for serviceability limit states

$\gamma_{f,ULS}$ = partial coefficient of the material for ultimate limit states

$\gamma_{f,SLS}$ = partial coefficient of the material for serviceability limit states

$f_{t,d,ULS}$ = design value of the longitudinal tensile strength, for ultimate limit states

$f_{t,d,SLS}$ = design value of the longitudinal tensile strength, for serviceability limit states

$A_{net}$ = net area of the cross-section with holes

$N_{t,Rd,ULS}$ = design value of the tensile strength of the profile

$f_{c,d,ULS}$ = design value of the compressive strength of the material

$N_{c,Rd,ULS}$ = design value of the compressive strength of the profile

$M_{2,Rd,ULS}$ = design value of the flexural strength of the profile for flexure around axis 2

$M_{3,Rd,ULS}$ = design value of the flexural strength of the profile for flexure around axis 3

$f_{V,Rd}$ = design value of the shear strength of the material

$V_{2,Rd,ULS}$ = design value of the shear strength of the profile in direction 2

$V_{3,Rd,ULS}$ = design value of the shear strength of the profile in direction 3

$L$ = length of the member

$M_0$ = value of the banding moment at the beginning of the member

$M_A$ = value of the banding moment at 1/4 of the length of the member

$M_B$ = value of the banding moment at 1/2 of the length of the member

$M_C$ = value of the banding moment at 3/4 of the length of the member

$M_1$ = value of the banding moment at the end of the member

$\left(f_{loc,k}^{axial}\right)_f$ = critical stress of the flanges, for stability verifications of compressed double-T profiles

$k_c$ = coefficient used for the stability verifications of compressed double-T profiles

$\left(f_{loc,k}^{axial}\right)_w$ = critical stress of the web, for stability verifications of compressed double-T profiles

$f_{loc,d}^{axial}$ = local critical stress, for stability verifications of compressed double-T profiles

$N_{loc,Rd}$ = design value of the compressive force that causes local instability of a double-T profile

$N_{Eul}$ = Euler buckling load

$\lambda$ = slenderness, used for the stability verifications of compressed double-T profiles

$\Phi$ = coefficient used for the stability verifications of compressed double-T profiles

$k$ = coefficient used for the stability verifications of compressed double-T profiles

$N_{c,Rd2}$ = design value of the force that causes buckling of a compressed double-T profile

$N_{c,Rd2,glob}$ = buckling load taking into account shear deformability

$R$ = coefficient used in the elements of the bending stiffness matrix of a plate

$D_{11,f}$ = element of the bending stiffness matrix of a plate

$D_{11,w}$ = element of the bending stiffness matrix of a plate

$D_{22,f}$ = element of the bending stiffness matrix of a plate

$D_{22,w}$ = element of the bending stiffness matrix of a plate

$D_{12,f}$ = element of the bending stiffness matrix of a plate

$D_{12,w}$ = element of the bending stiffness matrix of a plate

$D_{66,f}$ = element of the bending stiffness matrix of a plate

$D_{66,w}$ = element of the bending stiffness matrix of a plate

$\left(N_{x,cr}\right)_{f,box}^{SS}$ = local buckling load of the flange of a box-section profile

$\left(N_{x,cr}\right)_{w,box}^{SS}$ = local buckling load of the web of a box-section profile

$\left(N_{x,cr}\right)_{f,C}^{SS}$ = local buckling load of the flange of a C-section profile

$\left(N_{x,cr}\right)_{w,C}^{SS}$ = local buckling load of the web of a C-section profile

$\left(N_{x,cr}\right)_{f,L}^{SS}$ = local buckling load of the flange of a L-section profile

$\left(N_{x,cr}\right)_{w,L}^{SS}$ = local buckling load of the web of a L-section profile

$N_{c,Rd2,loc}$ = design value of the local buckling strength

$k_f$ = coefficient used for the stability verifications of double-T profiles subjected to bending

$\left(f_{loc,k}^{flex}\right)_w$ = value of the critical stress of the web of double-T profiles subjected to bending

$f_{loc,d}^{flex}$ = design value of the stress that causes local buckling of a double-T profile subjected to bending

$M_{loc,Rd}$ = design value of the bending moment that causes local instability of a double-T profile subjected to bending

$J_\omega$ = warping constant of a double-T profile

$M_{FT}$ = critical bending moment for flexural-torsional buckling of double-T profile

$\lambda_{FT}$ = coefficient used in flexural-torsional buckling verifications of double-T profiles

$\Phi_{FT}$ = coefficient used in flexural-torsional buckling verifications of double-T profiles

$\chi_{FT}$ = coefficient used in flexural-torsional buckling verifications of double-T profiles

$M_{Rd2}$ = design value of the critical bending moment for double-T profiles

$M_{\max}$ = maximum value of the bending moment in a member

$M_m$ = mean value of the bending moment in a member

$M_{eq}$ = equivalent bending moment

$C_b$ = coefficient used in flexural stability verifications

$L_b$ = unbraced length of a member subjected to bending

$M_{Rd2,glob}$ = design value of the global buckling strength of a member subjected to bending

$\left(N_{x,cr}\right)_{f,box}^{SS}$ = buckling load of the flange of a box-section profile subjected to bending

$\left(N_{x,cr}\right)_{w,box}^{SS}$ = buckling load of the web of a box-section profile subjected to bending

$\left(N_{x,cr}\right)_{f,C}^{SS}$ = buckling load of the flange of a C-section profile subjected to bending

$\left(N_{x,cr}\right)_{w,C}^{SS}$ = buckling load of the web of a C-section profile subjected to bending

$M_{Rd2,loc}$ = design value of the local buckling strength of a member subjected to bending

$K$ = coefficient used for the stability verifications of members subjected to shear

$f_{V,loc,k}$ = characteristic value of the tangential stress that causes local buckling in the web panel

$V_{Rd2}$ = design value of the shear force that causes local buckling of the member

$\alpha$ = coefficient used for the computation of the warping constant of C-section profiles

$J_{\omega,C}$ = warping constant of C-section profiles

$M_{Rd2,glob,C}$ = design value of the bending moment that causes global buckling of C-section profiles

$N_{c,Rd2,comp}$ = design value of the buckling strength, for compression and flexure stability verifications

$M_{Rd2,comp}$ = design value of the buckling strength, for compression and flexure and shear and flexure stability verifications

$N_{Eul,2}$ = Euler buckling load, for stability verifications of member subjected to axial force and bending moment

$\phi_E(t)$ = creep coefficient for axial strains

$\phi_G(t)$ = creep coefficient for shear strains

$E_L(t)$ = long-term value of the longitudinal elastic modulus

$G(t)$ = long-term value of the shear modulus

$f_{c,d,SLS}$ = design value of the compressive strength, for serviceability limit states

$f_{V,Rd,SLS}$ = design value of the shear strength, for serviceability limit states

To facilitate the reader and the designer much of the symbology adopted is equal to that of CNR-DT205/2007.

## 4.3. **Verification's functions**

V1= tensile stress (ULS)

V2= compressive stress (ULS)

V3= flexural stress 22 (ULS)

V4= flexural stress 33 (ULS)

V5= flexure 22 - compression stress (ULS)

V6= flexure 22 - tension stress (ULS)

V7= flexure 33 - compression stress (ULS)

V8= flexure 22 - tension stress (ULS)

V9= shear 2 stress (ULS)

V10= shear 3 stress (ULS)

V11= flexure 33 - shear 2 stress (ULS)

V12= flexure 22 - shear 3 stress (ULS)

V13= torsional stress (ULS)

V14= global buckling - compression (ULS)

V15= local buckling - compression (ULS)

V16= global buckling - flexure (ULS)

V17= local buckling - flexure (ULS)

V18= shear buckling (ULS)

V19= buckling - compression and flexure (ULS)

V20= buckling - shear and flexure (ULS)

V21= tensile stress (SLS)

V22= compressive stress (SLS)

V23= shear 2 stress (SLS)

V24= shear 3 stress (SLS)

V25= flexural stress 22 (SLS)

V26= flexural stress 33 (SLS)

V27= torsional stress (SLS)

V28= axial force and flexure 22 stress (SLS)

V29= axial force and flexure 33 stress (SLS)

V30 = maximum deflection (SLS)

## 4.4. **References**

Bank LC. Composites for construction-structural design with FRP materials, John Wiley & Sons, NJ, 2006.

CEN TC250 WG4L, Ascione, J-F. Caron, P. Godonou, K. van IJselmuijden, J. Knippers, T. Mottram, M. Oppe, M. Gantriis Sorensen, J. Taby, L. Tromp. Editors: L.Ascione, E. Gutierrez, S. Dimova, A. Pinto, S. Denton. 'Prospect for New Guidance in the Design of FRP,' Support to the implementation and further development of the Eurocodes, JRC Science and Policy Report JRC99714, EUR 27666 EN, European Union, Luxembourg, (2016), p 171. ISBN 978-92-79-54225-1 doi:10.2788/22306

CNR-DT205/2007 Guide for the design and constructions of structures made of FRP pultruded elements, National Research Council of Italy, Advisory Board on Techincal Recommendations. http://www.cnr.it/sitocnr/IlCNR/Attivita/NormazioneeCertificazione/DT205_2007.html.

Kollar L.P., Local Buckling of Fiber Reinforced Plastic Composite Structural Members with Open and Closed Cross Section. Journal of Structural Engineering, ASCE, 2003. 129: 1503-1513.

Eurocode 3: Design of steel structures - Part 1-1: General rules. ENV 1993-1-1: 1992. Incorporating Corrigenda February 2006 and March 2009.

SAP2000 Advanced v. 10.1.2. Structural Analysis Program, Computers and Structures, Inc., 1995 University Ave, Berkeley, CA.

Tarjan, G., Sapkas, A. and Kollar, L.P. Local Web Buckling of Composite (FRP) Beams. Journal of Reinforced Plastics and Composites, Vol. 29, No. 10/ 2010.

Tarjan, G., Sapkas, A. and Kollar, L.P. Stability Analysis of Long Composite Plates with Restrained Edges Subjected to Shear and Linearly Varying Loads, J. of Reinf. Plastics and Comp., Vol. 29, No. 9/ 2010.